aerospace

MDPI

Review

A Review of Novel Heat Transfer Materials and Fluids for Aerospace Applications

Glauco Nobrega [1,2], Beatriz Cardoso [1], Reinaldo Souza [1,3,*], José Pereira [3], Pedro Pontes [3], Susana O. Catarino [4,5], Diana Pinho [4,5], Rui Lima [1,6,7] and Ana Moita [3,8]

1 Mechanical Engineering and Resource Sustainability Center (MEtRICs), Mechanical Engineering Department, University of Minho, Campus de Azurém, 4800-058 Guimarães, Portugal; glaucotvn@hotmail.com (G.N.); beatrizdiascardoso94@gmail.com (B.C.); rl@dem.uminho.pt (R.L.)
2 Centro de Investigação de Montanha (CIMO), Campus de Santa Apolónia, Instituto Politécnico de Bragança, 5300-253 Braganca, Portugal
3 IN+, Center for Innovation, Technology and Policy Research, Instituto Superior Tecnico, Universidade de Lisboa, Av. Rovisco Pais, 1049-001 Lisboa, Portugal; sochapereira@tecnico.ulisboa.pt (J.P.); pedrodanielpontes@outlook.pt (P.P.); anamoita@tecnico.ulisboa.pt (A.M.)
4 Microelectromechanical Systems Research Unit (CMEMS-UMinho), School of Engineering, University of Minho, Campus de Azurém, 4800-058 Guimarães, Portugal; scatarino@dei.uminho.pt (S.O.C.); diana.pinho@cmems.uminho.pt (D.P.)
5 LABBELS—Associate Laboratory, Campus de Gualtar, 4710-057 Braga, Portugal
6 Transport Phenomena Research Center (CEFT), Faculdade de Engenharia da Universidade do Porto (FEUP), Rua Roberto Frias, 4200-465 Porto, Portugal
7 Associate Laboratory in Chemical Engineering (ALiCE), Faculty of Engineering, University of Porto, 4200-465 Porto, Portugal
8 CINAMIL—Centro de Investigação Desenvolvimento e Inovação da Academia Militar, Academia Militar, Instituto Universitário Militar, Rua Gomes Freire, 1169-203 Lisboa, Portugal
* Correspondence: reinaldo.souza@tecnico.ulisboa.pt

Abstract: The issue of thermal control for space missions has been critical since the early space missions in the late 1950s. The demands in such environments are heightened, characterized by significant temperature variations and the need to manage substantial densities of heat. The current work offers a comprehensive survey of the innovative materials and thermal fluids employed in the aerospace technological area. In this scope, the materials should exhibit enhanced reliability for facing maintenance and raw materials scarcity. The improved thermophysical properties of the nanofluids increase the efficiency of the systems, allowing the mass/volume reduction in satellites, rovers, and spacecraft. Herein are summarized the main findings from a literature review of more than one hundred works on aerospace thermal management. In this sense, relevant issues in aerospace convection cooling were reported and discussed, using heat pipes and heat exchangers, and with heat transfer ability at high velocity, low pressure, and microgravity. Among the main findings, it could be highlighted the fact that these novel materials and fluids provide enhanced thermal conductivity, stability, and insulation, enhancing the heat transfer capability and preventing the malfunctioning, overheating, and degradation over time of the systems. The resulting indicators will contribute to strategic mapping knowledge and further competence. Also, this work will identify the main scientific and technological gaps and possible challenges for integrating the materials and fluids into existing systems and for maturation and large-scale feasibility for aerospace valorization and technology transfer enhancement.

Keywords: nanomaterials; nanofluids; heat transfer; aerospace applications

Citation: Nobrega, G.; Cardoso, B.; Souza, R.; Pereira, J.; Pontes, P.; Catarino, S.O.; Pinho, D.; Lima, R.; Moita, A. A Review of Novel Heat Transfer Materials and Fluids for Aerospace Applications. *Aerospace* **2024**, *11*, 275. https://doi.org/10.3390/aerospace11040275

Academic Editor: Sergey Leonov

Received: 19 January 2024
Revised: 27 March 2024
Accepted: 28 March 2024
Published: 30 March 2024

1. Introduction

The inception of satellites, such as Explorer 1, has been a concerted effort to comprehend the dynamics of heat exchange in space and overcome the challenges inherent in

this environment. These challenges are far from straightforward, encompassing diverse sources of heat transmitted through radiation, abrupt temperature fluctuations in regions exposed to solar radiation or in shadowed areas, the absence of gravity, substantial thermal demands at combustion points, survival cell requirements, and the presence of heat hotspots in microprocessors, cameras, lasers, and other electronic equipment. As a result, the selection of materials and the arrangement of machine components must not only consider issues of weight and volume but also address the thermal control requirements across various surfaces of the systems [1,2].

Aerospace heat transfer enhancements require specific thermal management equipment. This is the case for heat exchangers that are designed for such demanding requirements and often require high performance. Hence, it is not uncommon to find heat exchangers utilizing the phase change phenomenon to efficiently remove heat, as exemplified by heat pipes widely employed in high-heat concentration areas. When temperature stability is crucial and a wide temperature range cannot be employed, phase change materials (PCMs) present a viable alternative. PCMs prevent overheating by transitioning from a solid to a liquid state, effectively acting as a heat accumulator when temperatures tend to decrease [3].

Conventional heat exchangers such as radiators are also utilized, either connected to heat pipes or through active systems, although the latter is avoided due to pump failure risks and vibrations that interfere with cameras and sensors [1]. The enhancement of these heat exchangers involves improving the thermal properties of fluids, and in this context, nanofluids (NFs) have emerged as a hot research field, as evidenced by worldwide research and publications. A nanofluid is a working fluid with a small volume fraction (5% or less) of solid components with nanoscale dimensions. The addition of these solid materials has a significant impact on the properties of the nanofluid, for example, in the convective and conductive heat transfer, specific heat, and rheology of the fluid [4].

Nanoparticles (NPs), nonetheless, are not limited to use just in NFs to improve the thermal properties: the use of nanomaterials for space applications is gaining increasing prominence, considering their potential to enhance specific properties at a molecular interaction level in resins, for instance, or to provide new optical properties. Certain nanoparticles can improve the ability to reflect light on surfaces constantly exposed to solar radiation. Simultaneously, they can increase emissivity in radiators. Additionally, nanomaterials in the coating can contribute to long-term radiation resistance [5,6]. Nanoparticles with higher thermal conductivity, such as metallic or graphene-based particles, enable better heat distribution in spacecraft structures, reducing the likelihood of overheating in regions more exposed to solar radiation [7–9]. In the case of heat generated by combustion, the opposite effect may be desired, where it is essential to prevent the heat from spreading throughout the entire spacecraft and concentrate it in a zone more resistant to heat. In this scenario, nanoparticles can contribute to reduce the thermal conductivity of the material, allowing the material to withstand higher temperatures without degradation and preventing the spread of potential flames [10,11].

In the present study, a review was conducted regarding the primary methods of temperature control in space vehicles, employing fluids that are potential candidates for nanofluid applications. Nanofluids refer to fluids to which nanoparticles are added in a colloidal mixture. Furthermore, an exploration is undertaken into the utilization of nanomaterials in the aerospace sector, specifically focusing on thermal applications, with an emphasis on the used particles and the obtained key results. This review work is based on a literature review of more than one hundred available works. To the best of the authors' knowledge, this forthcoming article fills a literature gap by representing the inaugural review in the field, encompassing nanomaterials utilized for thermal control in space applications. There is no published work giving particular emphasis on the application of innovative materials and fluids in aerospace purposes. The authors considered this study a unique and detailed gathering of information, and such an amount of quality data should serve for future guidelines in the exploration of nanomaterials and nanofluids in these

scientific and technological areas for aerospace enrichment. The structure of the current review is described as follows: brief descriptions of the currently used and near-future promising available heat transfer models, methods, and solutions for aerospace applications are provided in Section 2. Section 3 describes the general use of novel nanomaterials in aerospace purposes. Section 4 focuses on the general use of nanofluids in aerospace applications. The main concluding remarks and perspectives towards heat transfer methodologies are presented in Section 5.

2. Thermal Control Applied in Aerospace

In the Introduction section of the present work, it was highlighted that the needs and challenges encountered in the aerospace industry are both diverse and formidable. The considerable temperature variations, the specific cooling requirements for microchips and electronic devices, as well as the imperative for isolating the combustion area, all demand meticulous control within stringent constraints of weight and space. The selected tools should not only maintain temperatures within appropriate ranges but also prevent significant temperature cycles that could lead to system failures [12].

Moving beyond the design considerations and the intended location of the Cosmo fleet, the primary tools employed for thermal control include heat exchanger devices, thermal protection mechanisms, and thermal accumulators. This section provides an overview of thermal control techniques applied in space, categorizing them into active and passive methods for clarity and comprehensiveness.

2.1. Aerospace Heat Transfer Equations and Dimensionless Groups

2.1.1. Ablation

Ablation heat transfer modeling involves understanding how heat is transferred during the process of ablation, which is the removal of material from a surface provoked by high-temperature situations like the re-entry into the Earth's atmosphere or combustion. The ablative insulators are used in aerospace applications to protect structural components from extreme conditions. The physical phenomena associated with ablation heat transfer involve, among others, material pyrolysis and surface ablation. The key equation for ablation heat transfer involves the balance between heat conduction, material decomposition, and pyrolysis gas permeation. It takes into account effects such as heat exchange and thermochemical surface erosion. A simplified one-dimensional equation for ablation heat transfer can be expressed by Equation (1):

$$\frac{\partial^2 T}{\partial x^2} = \frac{\rho C_p}{k} \cdot \frac{\partial T}{\partial t} + q \tag{1}$$

where T is the temperature, x is the spatial coordinate, ρ is the density of the material, C_p is the specific heat, k is the thermal conductivity, and q represents the energy generation rate.

2.1.2. Heat Transfer at High Speed

High-velocity effects on heat transfer play an important role in a lot of technical applications, like re-entry problems for space applications, for heat transfer at high velocities around gas turbine blades or in rocket engines. High-speed convection involves the conversion of mechanical energy into thermal energy, resulting in strong temperature variations in the fluid and changes in the properties of the fluid resulting from temperature variations. Moreover, the Mach number is a dimensionless group that characterizes the compressibility of the fluid, and for Mach numbers inferior to 0.3, the flow can be considered incompressible.

2.1.3. Rarefied Gas Heat Transfer

The behavior of heat transfer in rarefied gases is of increased interest due to their relevance for thermal design and management. For instance, there is a high degree of heat transfer between the surface of the outer wall of a launch vehicle and the atmosphere

during the blastoff when passing through near-space (20–100 km). The term rarefied means that the molecular mean free path is not small compared to a characteristic dimension. The parameter that describes the degree of rarefaction is the Knudsen number. For the purpose of defining the Knudsen number, it is important to choose a suitable characteristic mean free path and length. When the Knudsen number is very small, the number of collisions between the molecules in the vicinity of the body is considerable in comparison to the number of collisions between the molecules and the body. In this case, the usual continuum concepts are applicable, and the Navier–Stokes equations and the Fourier heat conduction law are valid. In the cases where the Knudsen number is large enough, the continuum concepts must be modified for calculating the heat transfer. At very high Knudsen numbers, where the number of collisions between the molecules and the heating surface is much greater than the number of collisions between the molecules, the flow is commonly designated as free-molecule flow. The heat transfer in the free-molecule regime is directly proportional to the gas density and is independent of the spacing between the walls when considering the flow between two walls or plates, while the heat transfer in the continuum flow regime is inversely proportional to the plate spacing and independent of the density. The ratio of the continuum to the free-molecule heat conduction is found to be proportional to the Knudsen number of the flow and is given by Equation (2):

$$\frac{q_c}{q_{fm}} = \frac{4\gamma\lambda}{(\gamma+1)\alpha Prh} \propto \frac{\lambda}{h} \propto Kn \tag{2}$$

where γ is the specific heat ratio, λ is the mean free path, and α is the overall accommodation coefficient between the plates. For the transition and slip regimes with the Knudsen number between 10 and 0.01, the heat transfer can be approximated as a function of the asymptotic processes of continuum heat transfer and free molecular heat transfer. Such an approximation has been demonstrated to be consistent with published experimental data on heat transfer via rarefied argon and helium [13]. The formula based on this approach is given by Tien and Cunnington [14] and can be expressed by Equation (3):

$$\frac{q}{q_{fm}} = \left(1 + \frac{q_{fm}}{q_c}\right)^{-1} = \left(1 + \frac{C}{kn}\right)^{-1}, \frac{q}{q_{fm}} + \frac{q}{q_c} = 1 \tag{3}$$

where $c = \alpha(\gamma + 1)Pr/4\gamma$ is a constant. Finally, the heat transfer, valid for an arbitrary Knudsen number, can be obtained and given by Equation (4):

$$q = -k\frac{T_1 - T_2}{h + 4\gamma\lambda/\alpha(\gamma+1)Pr} \tag{4}$$

2.1.4. Cryogenic Heat Transfer

Cryogenic heat transfer involves the transport of heat between solid materials and adjacent cryogenic fluids. The convective heat transfer can be given by the following expression, known by Newton's law of cooling, given by Equation (5):

$$Q = h(Ts - Tf) \tag{5}$$

where Q is the heat transfer rate in kW/m^2, h is the HTC, Ts is the temperature value of the solid, and Tf is the temperature value of the fluid. Taking a liquid nitrogen precooler, using helium gas as an example, the total heat transfer can be given by Equation (6):

$$Q = \dot{m}C_P(T_{in} - T_{out}) \tag{6}$$

where Cp is the specific heat capacity of helium, m is the helium mass flow rate, and T_{in} is the boiling temperature of helium. Also, assuming turbulent flow, the Nusselt number can be given by the Johannes correlation expressed by Equation (7):

$$Nu = 0.0259 Re^{4/5} Pr^{2/5} \left(\frac{T_s}{T_f} \right)^{-0.716} \tag{7}$$

2.1.5. Microgravity Heat Transfer

For low-gravity two-phase flow heat transfer, in addition to the most commonly used dimensionless groups of the Reynolds and Prandtl numbers, the effect of gravitational and surface tension forces on the arrangement of the vapor and liquid phases must also be considered. Also, the flow regime transitions proposed by Zhao and Rezkallah [15] should be incorporated to consider the impact of the flow regime alteration caused by reduced gravity on the two-phase heat transfer. Microgravity heat transfer and two-phase flow are dependent on the force balance between inertia forces and surface tension forces. Such a balance can be defined as a function of the Weber number, such that annular flow was shown to be present for a Weber number superior to 20 (inertia region), slug–annular flow for a Weber number between 1 and 20, and slug and bubbly flows for a Weber number inferior to 1 (surface tension region). Also, for a Reynolds number inferior to 2300 (laminar flow), there should be considered the dimensionless groups of the Graetz number Gz based on the liquid superficial velocity and properties, the ratio of the superficial velocities or the pseudo-void fraction, and the liquid Morton number Mo. The Graetz number can be determined by Equation (8):

$$Gz = \frac{D}{L} \cdot Re \cdot Pr \tag{8}$$

where Pr is the Prandtl number of the liquid phase, D is the diameter of the heating test section, and L is the length of the heating test section.

The Morton number can be given by Equation (9):

$$Mo = \frac{g \mu^4}{\rho \sigma^3} \tag{9}$$

where g is the gravitational acceleration, μ is the liquid dynamic viscosity, ρ is the density of the liquid, and σ is the surface tension coefficient. As seen in the above equation, the Morton number is strictly dependent on fluid properties and gravity. This incorporates the effects of gravitational forces and surface tension forces in the analysis of the heat transfer data. For Reynolds numbers superior to 2300, the Reynolds number, the liquid Froude number, and the Morton number should be considered. The Froude number, Fr, based on the liquid superficial velocity, can be expressed by Equation (10):

$$Fr = v \sqrt{gd} \tag{10}$$

where v is the liquid superficial velocity, g is the gravitational acceleration, and d is the equivalent diameter of the bubble.

2.2. Active Methods

In this section, one delves into the primary active methods employed in the study of heat transfer, particularly those explored in space technology. These methods necessitate auxiliary devices or systems that rely on external energy, such as pumps and power sources, to enhance or intensify thermal exchange. ATCSs, flow boiling, and radiators stand out. An ATCS is utilized when spatial thermal control is achieved through fluids or moving mechanisms or power. Flow boiling, frequently applied in space applications, serves to cool critical components, such as electronics, in spacecraft. Lastly, radiators are also

highlighted, serving to control heat emission and efficiently regulate the temperature of spacecraft components.

2.2.1. ATCSs

Each component present in devices operating in space is subject to extreme cycles of temperature gradients. For this reason, it is crucial that these components operate within an ideal temperature range. In situations like these, the thermal control of components in spacecraft, satellites, and even the equipment composing the International Space Station (ISS) requires the proper utilization and disposal of the internal heat generated by these different components. In these cases, the implementation of an ATCS becomes indispensable. Moreover, an ATCS is capable of handling high heat loads. When the heat loads generated exceed the thermal control capabilities of a passive system, an ATCS becomes the safest option to be used. ATCS comprises heaters, temperature sensors, and a thermal control computer (TCC) controlled by a computational routine based on one algorithm, as reported in Xiong et al. [16].

On the ISS, the ATCS used, according to a report provided by the National Aeronautics and Space Administration in 2021 [17], operates through a closed circuit, through which a mechanically pumped fluid passes. There are three functions for the ATCS: collecting, transporting, and rejecting heat. Excess heat can be removed in two ways: using heat exchangers or cold plates, both cooled by circulating ammonia circuits located outside the station. The report by NASA in 2021 [17] explains that, when heated, ammonia circulates through large radiators, releasing heat by radiation into space. The low temperature of this external environment cools the ammonia as it flows through the radiators.

Ungar and Erickson [18] described the ATCS employed in spacecraft for dissipating excess heat from electronic equipment and habitable areas. These systems can consist of single-loop configurations or dual-loop setups connected in series, known as double-loop systems. In single-loop systems, a single pumping circuit removes residual heat generated in the crew cabin and other spacecraft components, releasing it into the environment. Conversely, double-loop systems feature two distinct circuits, inside and outside the crew cabin, connected via an interloop heat exchanger. An ATCS typically operates redundantly to ensure fault tolerance, activating alternative systems if issues arise with one. Therefore, spacecraft utilizing single-loop configurations effectively have multiple parallel loops, while those employing double-loop setups boast several pairs of independent internal and external loops.

Moreover, Wang et al. [19] reported a significant reduction in the ATCS for spaceborne high-resolution remote sensors (HRSs), achieving a 78.6% reduction rate in the ATCS's resource occupancy. The authors employed an unsupervised learning framework integrating kernel-based principal component analysis with Gaussian mixture model clustering. The reconstructed ATCS maintained temperature fluctuations within a narrow range of $\pm$0.02–0.6 °C, while the optical performance was preserved. Notably, the thermal control system (TCS) cannot achieve the same level of thermal compensation as an ATCS. Also, the stringent temperature stability requirements of optical payloads, such as those in telescopes and space satellites, are crucial. Li et al. [20] and Meng et al. [21] emphasized that a failure to maintain temperature stability may lead to thermally induced deformations, resulting in the misalignment and distortion of optical surfaces and consequently the degradation of image quality. The latter demonstrates an analysis of the influence of imaging quality under a temperature load of 2 °C, revealing that the optical system's modulation transfer function (MTF) decreased by 2.36. Additionally, an analysis of imaging quality with a temperature difference generated by a 0 °C flange face and a 20 °C camera in orbit revealed that the MTF of the optical system decreased by 3.5. The thermal control system in the camera's thermal design showed that it could maintain its temperature above 10 °C in low-temperature storage mode and within 18–1 °C during working conditions, ensuring its operational reliability.

Figure 1 shows the interface of an active thermal control system used by NASA and international partners on the International Space Station. The ATCS consists of two basic systems, one internal and one external.

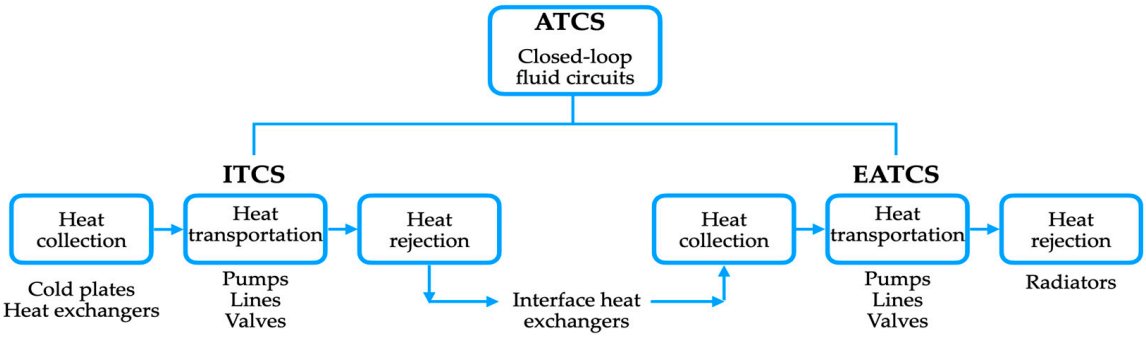

Figure 1. Active thermal control system framework. Adapted from [18].

The internal thermal control system (ITCS) has the function of keeping the equipment inside the habitable module operating within an acceptable temperature range and collecting, transporting, and rejecting residual heat. In this case, water is the fluid used to perform the task as it exhibits efficient thermal transport and is considered safe for use inside the habitable module.

On the other hand, the external active thermal control system (EATCS), being located on the external part of the space station, uses ammonia circuits to collect heat from interface heat exchangers and external electronic equipment mounted on cold plates. Afterward, it transports this heat to the radiators, which consist of two independent loops, one positioned in the starboard side and the other in the port side. Subsequently, the residual heat is rejected into space.

2.2.2. Flow Boiling

The flow boiling process is one of the most effective modes to achieve an enhanced heat transfer performance required for aerospace applications. This heat transfer process can be employed in a wide range of microgravity systems, including the cooling of electronic devices subjected to increased heat fluxes, communication satellites, thermal management of the International Space Station, the cooling of electronic devices subjected to high thermal loads, and the cooling of nuclear space reactors, among others. A profound understanding of all the influencing factors in low-gravity flow boiling is necessary to design and fabricate thermal management systems for space applications. Furthermore, the scientific communities of space exploration and heat transfer have been making significant efforts to develop high-performance rocket engine cooling channels.

In this context, Ortega et al. [22] reported the results of liquid nitrogen flow boiling for asymmetrically heated GR-Cop42 channels. The experiments were conducted at different mass flux pressures and subcooling degrees. A maximum departure from the nucleate boiling critical heat flux of 768 kW/m^2 was achieved for a 1.8 mm channel. The repeatability of flow boiling performance was inferred using the 1.8 mm × 1.8 mm cooling channel, showing a maximum CHF (critical heat flux) variation of ±1.1% at 57 cm^3/s and ±0.5% at 47 cm^3/s liquid nitrogen flow tests, which are significantly lower than the measurement uncertainty of ±2.5%. The effect of the nitrogen flow rate on the flow boiling heat transfer coefficient (HTC) and CHF was evaluated with a 2.3 mm × 2.3 mm channel (2.3 mm hydraulic diameter).

The HTC increased with an increasing mass flux in the range of 3824 $kg/m^2{\cdot}s$ to 8605 $kg/m^2{\cdot}s$. The same trend was observed with an increasing mass flow rate from 25 cm^3/s to 38 cm^3/s due to the contribution of enhanced nucleate boiling. However, with the liquid nitrogen flow rate increasing to 47 cm^3/s, the HTC decreased, interpreted as a suppression of nucleate boiling. Further increasing the flow rate to 57 cm^3/s resulted in

an appreciable contribution from forced convective evaporation, leading to a remarkable increase in the HTC.

Nonetheless, the CHF increased linearly with the growing mass flux due to the diminishing influence of flow instability and gravitation effects and the increasing forced convective evaporation. CHF values ranging from 337 kW/m^2 to 459 kW/m^2 were obtained at liquid nitrogen flow rates of 25 cm^3/s and 57 cm^3/s for the 2.3 mm channel, respectively.

The effect of pressure on the HTC and CHF was evaluated for the 1.8 mm × 1.8 mm (1.8 mm hydraulic diameter) and 1.8 mm × 4.1 mm (2.5 mm hydraulic diameter) channels at pressures of 1.38 MPa and 1.59 MPa, respectively. Increasing the pressure resulted in critical heat flux deterioration due to the reduction in surface tension and latent heat of vaporization of the liquid nitrogen. The CHF decreased by 13% (1.8 mm channel) and 14% (2.5 mm channel) with increasing pressure. However, the HTC increased with increasing pressure, attributed to the decreasing size of the bubbles and an increase in their departure frequency.

Moreover, among the three different channels, enhancements in CHF and HTC were achieved by reducing the channel size. The results showed that the CHF increased from 307 kW/m^2 to 752 kW/m^2 with a decreasing channel size from 2.5 mm to 1.8 mm, respectively, due to the considerably greater contribution of forced convective evaporation. A CHF enhancement from 548 kW/m^2 to 752 kW/m^2 was verified for the 1.8 mm channel with an increase in the liquid nitrogen flow rate from 47 cm^3/s to 57 cm^3/s. Figure 2 presents the cryogenic flow boiling test facility.

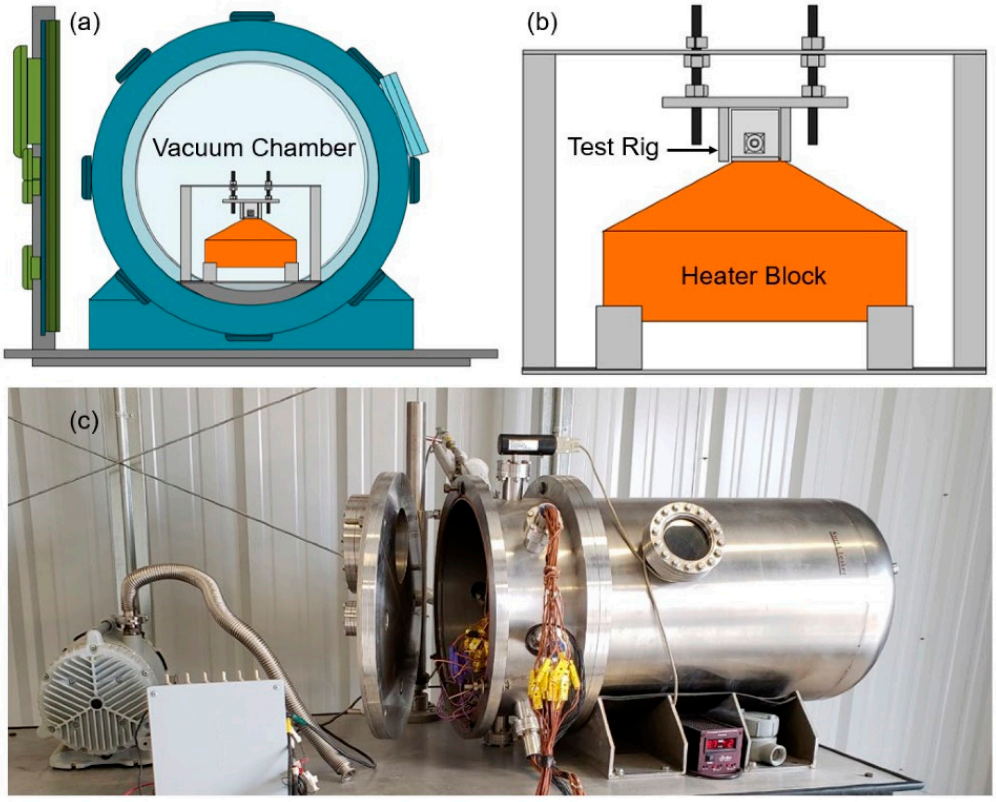

Figure 2. Cryogenic flow boiling test facility: (**a**) scheme of the assembly inside the vacuum chamber, (**b**) scheme of the test stand, test rig, and heater block assembly, and (**c**) test facility [22].

Inoue et al. [23] conducted flow boiling experiments on board the International Space Station, integrated into the Two-Phase Flow experiment promoted by JAXA. The goal of this experiment was to obtain valuable results for the thermal management of aerospace applications, including advanced satellite systems, space exploration, and manned space

activities. Microgravity data on two-phase flow and heat transfer in the flow boiling process with FC-72 were obtained using a copper heated test tube and a glass heated tube, with varying mass flux, liquid subcooling, and imposed heat flux.

The primary objective of the experiments they conducted was to elucidate the effect of gravity on flow boiling. To evaluate this impact, it is crucial to compare the heat transfer data and two-phase flow behaviors obtained in terrestrial gravity and microgravity environments under the same operating conditions. However, neither experiment could not be conducted with the same setup and experimental conditions. Additionally, consideration must be given to heat losses due to forced avionics air flow inside the experimental apparatus on the International Space Station. Therefore, the evaluation of fluid conditions at the inlet of the test tube required the development of a heat loss model.

The heat loss model for evaluating the degree of liquid subcooling at the inlet of the heated test tube and heat flux from the heated tube to the test fluid was developed using the results of preliminary heat loss experiments conducted on board the International Space Station. The authors concluded that the accuracy of the heat loss evaluation was improved by including correction factors for thermal resistance across thermal insulation material for each section and by developing a single-phase convection heat transfer correlation for the laminar–turbulent transition region. The difference in liquid subcooling at the inlet of the metal heated tube is less than 7.8 K, whether the exact heat loss model is considered or not. This correction is a significant factor in the accurate evaluation of gravity effects. In the analysis of a single-phase turbulent flow heating experiment conducted on board the International Space Station, it was confirmed that the estimated heat transfer coefficients using the heat loss model for the metal heated tube were almost the same as the calculated values from existing heat transfer correlations.

Devahdhanush et al. [24] conducted experiments on the flow boiling of n-perfluorohexane using a saturated two-phase mixture inlet in a rectangular channel. These experiments were integrated into the Mission Sequence Testing of the Flow Boiling and Condensation Experiment's Flow Boiling Module in the vertical up-flow configuration on Earth's gravity, using the same experimental system launched at the International Space Station in 2021. Adjusted working parameters included the option for single- and double-sided heating configurations, mass flux, and inlet pressure.

The obtained flow patterns were characterized by low-density and high-density fronts moving along the channel, with the high-density fronts gradually reducing in length due to the evaporation process. Critical heat flux results were combined with prior databases to create a consolidated Flow Boiling Condensation Experiment–CHF database for saturated inlet conditions, broadening the optimal operating conditions and incorporating other flow orientations in Earth gravity experiments.

The interfacial liftoff model exhibited good predictive accuracy for critical heat flux, as evidenced by an absolute error of nearly 12% for the database when restricted to mass fluxes superior to 500 $kg/m^2 \cdot s$. Figure 3 presents the single-sided heating configuration.

Mudawar and Lee [25] conducted a numerical investigation into the flow boiling process using n-perfluorohexane in microgravity on the International Space Station. The data for the analysis were acquired using the Flow Boiling and Condensation Experiment Flow Boiling Module, employing a rectangular channel with dimensions of 5.0 mm in height, 2.5 mm in width, and 114.6 mm in heated length. The results were analyzed for mass fluxes of approximately 200, 800, and 2400 $kg/m^2 \cdot s$ and heat fluxes corresponding to approximately 20%, 40%, and 60% of the CHF.

The detailed development of interfacial behavior was captured by a high-speed video through the channel's transparent sidewalls. In the computational fluid dynamics (CFD) model, the numerical solver was developed in ANSYS Fluent, combining the multiphase model with models for turbulence, surface tension, and interfacial phase change. Additionally, momentum source terms governing bubble shear lift, bubble drag, and bubble dispersion were incorporated.

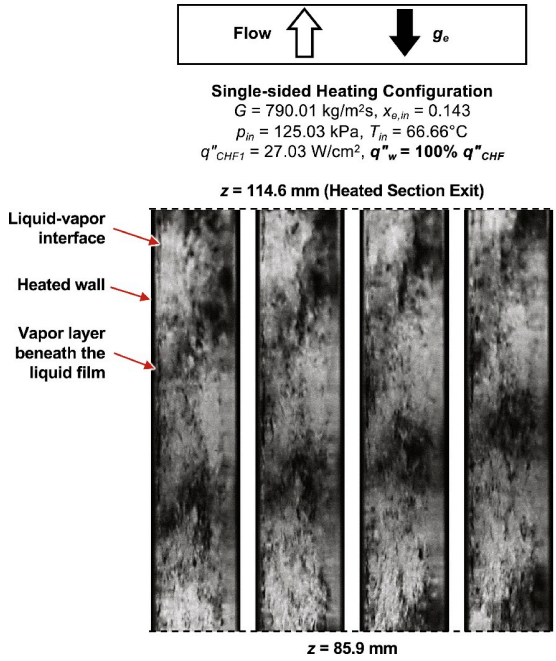

Figure 3. Single-sided heating configuration [24].

The accuracy of the predictions was assessed through a comparison against heat transfer data and the video-captured interfacial behavior. Very good agreement was attained against the measured axial profile of heated wall temperatures and further validated by video-capturing features such as vapor bubble generation, coalescence, departure, and vapor layer formation at the interface. Moreover, the CFD simulations enabled the estimation (not possible from experiments) of other relevant flow boiling factors like operating fluid velocity, mixture temperature, and cross-sectional profiles of void fraction.

The CFD model was based on the multiphase volume-of-fluid model along with phase change and turbulence models, enhanced with the inclusion of forces linked with surface tension, shear lift on bubbles, drag, and bubble collision dispersion.

The authors concluded that at mass fluxes of 199.9, 799.9, and 2399.9 kg/m^2·s, bubble nucleation remained along the heated length at heat fluxes corresponding to around 20% and 40% of the critical heat flux. For the two lower mass fluxes, increasing the heat flux to around 60% of the critical heat flux resulted in significant bubble coalescence and the formation of large, elongated bubbles and vapor layers, especially downstream. High flow inertia at G = 2399.9 kg/m^2·s greatly reduced both bubble growth and coalescence for all heat fluxes. The model also demonstrated good accuracy in predicting the interfacial behavior and heat transfer data.

For the considered mass fluxes and heat fluxes, the measured and predicted wall temperatures were uniform along the heated length, albeit with slightly lower values in the entrance and exit regions. The lower temperatures upstream were attributed to the creation of a thin upstream thermal boundary layer where single-phase cooling was appreciable, and two-phase cooling was not fully developed. The lower temperatures downstream were the result of enhanced heat transfer resulting from the acceleration of the fluid.

The determination of the HTC depended on the heat flux boundary along the heating walls, using either local heat flux passing through the copper–fluid interface or constant heat flux. The estimated values for the HTCs showed good agreement throughout most of the heated length. Figure 4 schematically represents the configuration of the numerical simulation.

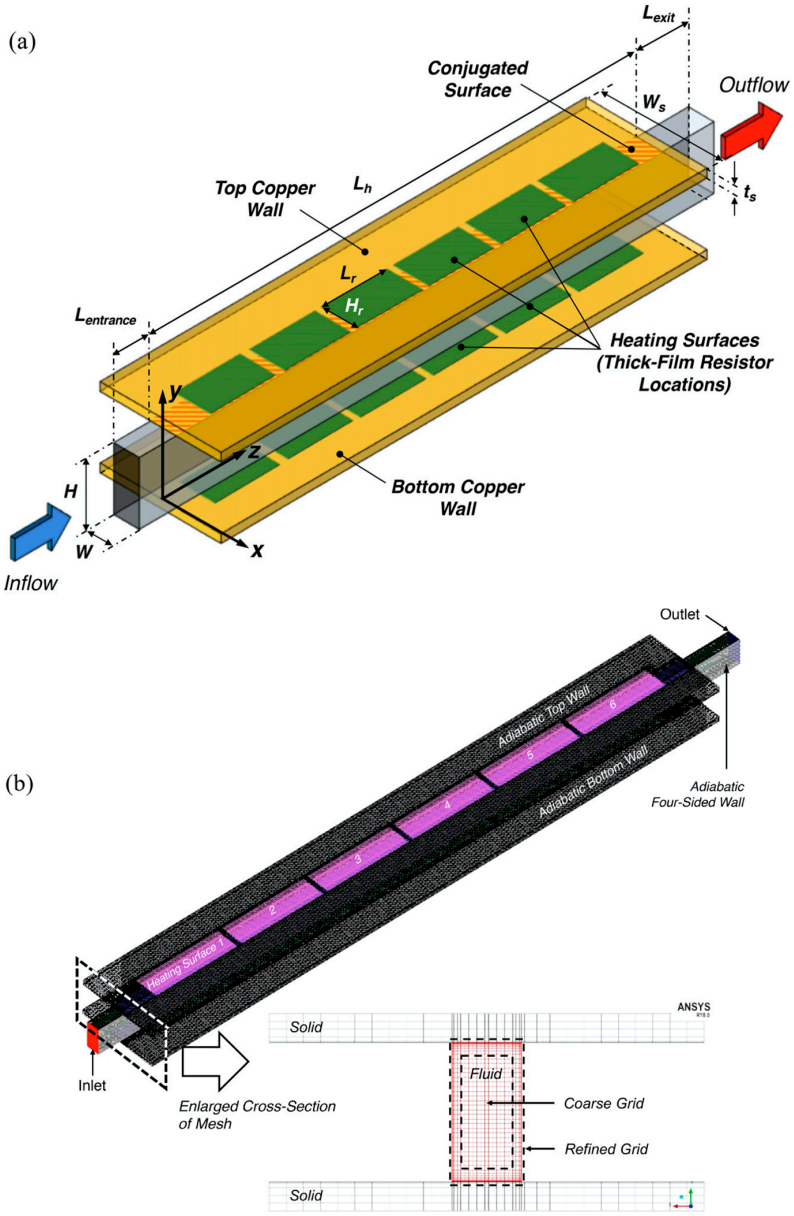

Figure 4. Scheme of the configuration of the numerical simulation: (**a**) Three-dimensional computational geometry and (**b**) Mesh configuration in full domain and cross-section area [25].

2.2.3. Radiators

The space nuclear power system can operate stably in extreme environments, with high output power, high energy density, a small specific area, long working hours, autonomy, and system reliability [26]. The high-power space nuclear reactor system requires significant heat dissipation, making the radiator the component with the largest weight proportion in the heat dissipation system and the most substantial part of the space nuclear-powered spacecraft. The volume of the heat dissipation component typically represents nearly 60% of the spacecraft, and the space radiator accounts for approximately 40% of the spacecraft's weight [27]. The weight of the radiator significantly contributes to the total weight of the spacecraft, impacting both the launch weight and the feasibility of engineering development [28].

The radiator comprises thermal conductive and insulation materials to ensure an enhanced heat transfer performance. Additionally, fluid circuit radiators, heat pipe radiators, solid particle radiators, and strip radiators are among the most common aerospace radiators. In particular, the heat pipe space radiator offers significant advantages in heat transfer

capability, temperature regulation, and anti-collision issues. It has been successfully applied to spacecraft thermal control systems, demonstrating valuable practical application. The increasing presence of space debris raises the likelihood of the spacecraft radiator system encountering debris, and the risk of micrometeoroid impacts has significantly risen, imposing higher requirements for spacecraft heat dissipation. With the assistance of heat pipe and radiation panel technology, the heat pipe radiator demonstrates improved efficiency, engineering feasibility, enhanced heat transfer, and anti-debris impact performance.

Furthermore, the authors Lee et al. [29] reported that for future space transportation and planetary exploration mission power applications, NASA's Glenn Research Center is currently developing a nuclear fission system (Kilopower system) with an operable range between 1 kW and 10 kW and a lifespan of 8 years to 15 years. The thermal management of the Kilopower system involves high-temperature alkali metal heat pipes to transport heat from the nuclear reactor to Stirling convertors. Titanium water heat pipes are also utilized to remove waste heat from the converters' cold end and transport it to the radiators for rejection into space.

The titanium water heat pipes feature a special wick structure design, comprising a porous screened evaporator and a screen–groove hybrid wick in the adiabatic and condenser sections. These heat pipes can operate in space with zero gravity on planetary surfaces with gravity-aided orientation and on the ground with a slight adverse gravity orientation. Additionally, the heat pipes have the capacity to start up smoothly after being frozen. Various freeze/thaw-tolerant heat pipes were developed, manufactured, and tested in a thermal vacuum chamber. The results obtained demonstrated that the titanium heat pipes, with attached radiators, were able to transfer the required power at 400 K in space-like conditions, exhibiting a thermal resistance of 0.019 °C/W. The weight of the heat pipe radiator was less than 0.73 kg.

Moreover, Li et al. [30] performed sensitivity analysis and a double-objective optimization of parameters affecting the weight and heat dissipation area of a sodium–potassium alloy heat pipe radiator designed for use in space nuclear propulsion spacecraft, with a power range of 200 kW to 500 kW. The velocity field and temperature field of the heat pipe radiator were simulated and analyzed using ideal design parameters. The researchers determined the heat distribution of a two-dimensional fin model through an iterative finite difference method. They also investigated the impact of fin width (w), inlet temperature (T), length of the condensation section (l), and mass flow rate (q_m) on the heat pipe radiator weight (M) and heat dissipation area (A).

The optimization algorithm provided optimal design parameters, yielding values of approximately w = 0.09 m, T = 699.9 K, l = 0.80 m, q_m = 9 kg/s, M = 320.6 kg, and A = 18.07 m^2. The authors concluded that, influenced by wall friction resistance, the velocity in the middle of the pipe was the highest, with the velocity at the wall boundary approaching zero. The velocity was nearly equal on the sodium–potassium pipe with an equal distance from the center line of the coolant pipe, indicating high fluid flow ability. The temperature on the central line of the coolant pipe was the highest, while the temperature near the heat pipe evaporation section was lower. The temperature in the fin near the evaporation and condensation sections was superior to that further away. The researchers suggested that designing the fin shape along the isotherm could effectively improve the heat transfer efficiency of the radiator.

The solid particle radiator utilizes a stream of solid particles to radiate waste heat and dissipate it into space. In comparison to the liquid droplet radiator, this type of radiator possesses several advantageous features, including a reduction in the rate of mass per unit power, the avoidance of contamination from losses by evaporation, and a wide variation in radiating temperature without considering evaporation loss. Additionally, it is lightweight, occupies a small volume, presents an extended radiating surface, and exhibits a high rate of heat rejection.

The authors, Zhao et al. [31], conducted a mass model and parameter analysis to infer the performance of the solid particle radiator in diverse conditions. An optimization

calculation procedure was followed to minimize the solid particle radiator mass per unit power as a function of the average solid particle temperature at the collector. The researchers concluded that the total rate of mass per unit power was lower than that of the heat pipe radiator and liquid droplet radiator in most cases, under both conditions of environmental temperature at 300 K and 1000 K. The temperature of the solid particle stream varies to a larger extent when evaporation losses are not considered. Furthermore, the temperature of the solid particle stream strongly influences the rate of mass per unit power. The emissivity value of the solid particle also affects the rate of mass per unit power in different cases at 300 K. The rate of mass per unit power decreases with an increase in emissivity. The material selected for the solid particle is relevant as the specific heat impacts the number of rates of mass per unit of power. It was found that the rate decreases with increasing specific heat. The obtained results showed that the solid particle radiator not only yields no contamination into space environments and installations but also has the potential to significantly reduce the weight of spaceborne systems. Thus, the applications of heat rejection in space with this configuration should be further considered and thoroughly investigated.

2.3. Passive Methods

This section will provide a brief description of some options, which many consider among the most interesting from the perspective of heat transfer related to passive methods. These methods explore natural principles, properties, and material geometry to facilitate the movement of heat from one region to another, without the need for the use of energy from an external active source to perform such a transfer. For this purpose, some examples of systems were explored: heat pipes, PCM, and pool boiling. As will be seen in the following, these systems can operate independently or be integrated with another piece of technology.

2.3.1. Heat Pipe

Heat pipes are efficient heat transfer devices that operate based on the principles of phase change. They consist of a hermetic enclosure containing a working fluid. When one end of the pipe is heated, the fluid evaporates, moving to the other cold end, where it condenses and releases this heat. Figure 5 below shows the operating principle of the device. Its thermal conductivity is significantly high and can reach up to 100 times the conductivity of copper [32]. Furthermore, according to Kianfar et al. [32], the device's uniform temperature distribution, simple structure, affordable price, and passive operation make it attractive in various applications ranging from computer cooling systems [33], solar panels [34], and solar transformers [35] to the aerospace industry.

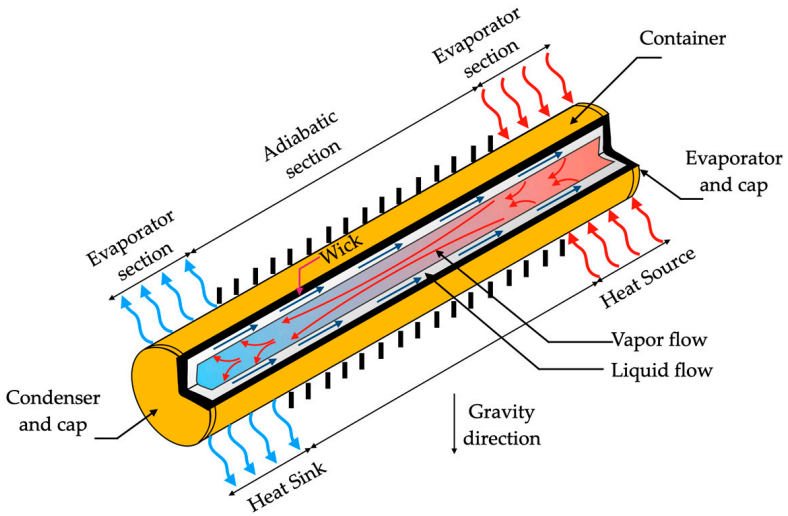

Figure 5. Schematic drawing showing the working principle of a heat pipe.

There are heat pipes with specific applications, the most common being the following: flat heat pipe, diode heat pipe, thermosyphon, variable conductance heat pipe (VCHP), and constant conductance heat pipe (CCHP). In relation to space applications, heat pipes have been used for at least five decades. In 1975, for example, Mock et al. [36] used a variable conductance heat pipe system that was designed to provide thermal control for an experimental transmitter package to be carried on a communications technology satellite.

Integrating a heat pipe (HP) and solid–liquid phase change material (PCM), for example, Kim et al. [37], using mathematically developed models specifically for numerical analysis, managed to propose a new thermal control hardware for spacecraft, reducing the complexity of the elements used. In the study in question, they demonstrate that integrating PCM into the heat pipe, with just a small addition of mass, less than 10% of the total radiator mass, provides a reduction in the operational temperature of the component by 28 °C.

Recently, Zhao et al. [38] conducted a review on the main working fluids and the effects of flow state on the thermal performance of microchannel oscillating heat pipes (MCOHPs) for aerospace purposes. The researchers concluded that the exploration of graphene nanofluids as heat transfer fluids can reduce thermal resistance by 83.6%, leading to an increase in thermal conductivity of almost 105%. The authors also reported that the working stage alters the heat flow pattern, affecting the oscillating heat pipe's flow mode and heat transfer capacity. Furthermore, they noted that the effective thermal conductivity varies from 4.8 kW/(m·K) to 70 kW/(m·K), depending on the use of different working fluids flowing through the heat pipe.

Ababneh et al. [39] tested the application of copper–water and aluminum–ammonia heat pipes for electronic heat dissipation in terrestrial and aircraft systems. Advanced Cooling Technologies Inc. (ACT)—1046 New Holland Ave, Lancaster, Pennsylvania 17601, USA, in collaboration with NASA's Marshall Space Flight Center and the International Space Station office at NASA's Johnson Space Center, conducted tests on heat pipes in space. The heat pipes were embedded in a high-conductivity HiK™ aluminum plate and subjected to thermal tests ranging from −10 °C to 38 °C for 10 days. The results showed excellent agreement with predictions and ground tests.

In this study, high-heat-flux constant conductance heat pipes based on hybrid wick technology were developed, overcoming the 5–10 W/cm^2 limitation of traditional grooved heat pipes in space applications. Two high-heat-flux hybrid CCHPs, HHF1 and HHF2, were created and tested. HHF1 transported a heat load exceeding 320 Watts with a heat flux exceeding 50 W/cm^2 and a thermal resistance below 0.012 °C/W, as confirmed by Lockheed Martin. HHF2 carried a heat load of 275 Watts with a heat flux exceeding 50 W/cm^2 and a thermal resistance of 0.015 °C/W at a 0.25 cm adverse elevation. This demonstrated a 3-fold heat flux capability enhancement over the standard aluminum–ammonia constant conductance design.

The results indicate that the heat pipe performs efficiently, consistently, and reliably, adapting to various high-heat-flux applications. These devices offer comprehensive thermal solutions for systems, including the spot cooling of electronic devices with space-qualified copper–water heat pipes, effective heat spreading of electronic boards and enclosures with space-qualified HiK™ plates, and efficient heat transport outside the electronics control box using constant conductance heat pipes.

Hu et al. [40] proposed the use of high-temperature sodium–GH4099 heat pipes for space reactor cooling due to their impressive thermal performance. These devices exhibit strong resistance to single-point failure, ensuring safety and self-actuating operation. The researchers analyzed the startup properties and thermal performance of the developed heat pipe. They concluded that the startup temperature of sodium/GH4169 heat pipes was approximately 620 °C. During startup tests, the fabricated heat pipes were successfully initiated at a heating temperature of 950 °C, reaching a temperature of nearly 800 °C. The charging ratio significantly impacted the startup properties of sodium–GH4099, with reported startup failures at sodium charging ratios of 24% and 30%, respectively.

Under simulated space reactor conditions, the axial temperatures of pre-oxidized sodium–GH4099 heat pipes were found to be lower than the end-use temperature of the GH4099 alloy. This indicates that pre-oxidized sodium–GH4099 heat pipes hold promise as alternatives for space reactor cooling.

Moreover, the pulsating heat pipes have also been used in microgravity conditions. In this sense, a research team, supported by the Japanese Space Agency, proposed the analysis of the heat transfer performance of flat-plate pulsating heat pipes through parabolic flights [41]. The results indicated that the pulsating heat pipe could work under reduced gravity. Corroborating this finding, an investigation team supported by the European Space Agency evaluated a tubular pulsating heat pipe and verified that for a planar geometry, the operation of a capillary pulsating heat pipe in microgravity was like the horizontal operation on ground. The Japanese investigation team, supported by the Japanese Space Agency, proposed the testing of a flat-plate pulsating heat pipe on orbit with a long-duration experiment, starting in 2012, showing that the heat transfer behavior was similar to that attained from ground experiments without any deterioration for a period of approximately four years [42]. Also, the absence of buoyancy forces acting on the operating fluid in weightless scenarios gave the opportunity to design and implement an innovative solution based on the use of a large diameter pulsating heat pipe that operates as a hybrid thermal management system between a two-phase loop thermosyphon in the presence of a gravity field and a pulsating heat pipe under microgravity, enabling the ability to strongly reduce the losses from viscosity and enhance the heat load ability, making it very suitable for high-power systems. The experiments, conducted and supported by the European Space Agency demonstrated that such combined systems worked as a loop thermosyphon on the ground and then, under microgravity conditions, switched to the pulsating heat pipe functioning [43]. As a future challenge, and given that fluid flow can also be influenced by viscosity and inertia, such issues should be further in-depth studied under prolonged microgravity. Also, it is noteworthy to mention that an international research team is working together with the European Space Agency to evaluate a large-diameter pulsating heat pipe onboard the International Space Station in 2024.

2.3.2. Phase Change Materials (PCMs)

Due to their ability to store large amounts of latent heat during phase transitions without experiencing a significant temperature change, phase change materials (PCMs) are extremely effective in applications that require temperature control and thermal management. Their applications are diverse: in solar thermal energy [44], they store heat collected during the day to release it at night, ensuring a continuous supply of thermal energy; as thermal insulation [45], they help maintain constant temperatures in buildings, packaging, and other devices, reducing the need for heating and cooling systems; in the thermal management of electronic devices [46], PCMs are incorporated into electronic components to absorb and dissipate excess heat, maintaining stable temperatures and preventing damage from overheating; and in the aerospace industry [47], they are used in the thermal control of spacecraft.

Nonetheless, conventional phase change materials possess low thermal conductivity and a high expansion ratio during phase change, and they entail the risk of leakage. These factors have prompted the scientific community in the field to focus on the search for novel phase change materials as part of phase change temperature control technology. This includes the use of microcapsules containing phase change materials and high-porosity foam metal materials [48].

Microencapsulated phase change materials involve the use of film-forming materials to wrap solid, liquid, or gas into very small particles. The latent heat of the phase change material in the microcapsule enhances the heat storage ability of the composite material significantly, thereby improving the heat storage capability of the systems. NASA employs microencapsulated phase change materials in spinning to create temperature-regulated space suits.

High-porosity foamed metal materials can achieve an 8-fold thermal conductivity enhancement of the composite phase change materials when filled in. In general, aerospace applications under periodic high-amplitude thermal cycles will significantly benefit from phase change materials temperature control systems.

In the case of deep space and planetary exploration spacecraft, thermal environments undergo much higher fluctuations than orbital spacecraft. For the latter case, it is more important to dissipate heat during hot operating phases and maintain the required temperature range for safe system operation in cold environments. A relevant concern is the heat rejection system that dissipates heat into space.

According to Collette et al. [47], the application of PCMs on planetary missions is not a novelty. In the 1970s, NASA conducted studies on various phase change materials to gather relevant information for the thermal control of spacecraft. During this period, three PCMs were identified as suitable: lithium nitrate with zinc hydroxyl nitrate catalyst, acetamide, and myristic acid.

Concerning space applications, two of the main constraints are weight and volume. In this context, Lafdi et al. [49] attempted to design phase change material thermal management systems under weight and volume constraints, aiming for the maximum storage capacity-to-volume ratio under dynamic thermal loads. The authors conducted a numerical investigation to estimate the thermal behavior of graphite foams with varying levels of porosity infiltrated with phase change materials for space applications. The researchers found that the average output power increased by more than eight times.

On the other hand, He et al. [50] developed a model for a photovoltaic phase change material–thermoelectric coupling system to study energy transfer and conversion in the aerospace environment. The phase change material was integrated into the system in pure form as well as in a metal foam composite phase change material. Considering power generation efficiency and system mass as a critical evaluation index for space systems, a combined performance criterion was defined. The average total efficiencies for the photovoltaic–thermoelectric, photovoltaic phase change material–thermoelectric, and photovoltaic–metal foam composite phase change material–thermoelectric systems were around 29.5%, 30.5%, and 30.6%, respectively. The corresponding average power densities were nearly 30.3 W/kg, 22.4 W/kg, and 21.2 W/kg, respectively. The research team stated that the mass of the ceramic layer and phase change material layer had the greatest impact on the total mass of the photovoltaic phase change material–thermoelectric system. The authors concluded that reducing the mass of the ceramic layer and exploring a high melting enthalpy phase change material were effective strategies to diminish the mass of the photovoltaic phase change material–thermoelectric-integrated system and promote its use in space applications.

Recently, Kachalov et al. [51] utilized a phase change material (PCM) to maintain a suitable and habitable temperature within a space habitat, isolating it from external solar radiation. The study considered integrating the PCM into the walls of the habitat. The system was analyzed through numerical simulation, considering heat transport only through diffusion (conduction), representing a scenario close to real microgravity or reduced gravity environments. Parameters such as the length of the PCM cell and thermal and optical properties of the external wall were considered in the study. The simplified one-dimensional model developed by the authors simulated periods of illumination and eclipse. They managed to demonstrate that, for a specific choice of PCM, geometry, and solar cycle, there exists an optimal absorptivity–emissivity ratio capable of maintaining the internal temperature of the habitat passively. Figure 6 presents a schematic illustration of a generic PCM integrated in a spacecraft radiator and the associated heat transfer mechanisms. Figure 7 schematically represents the applications of a PCM in electronic devices.

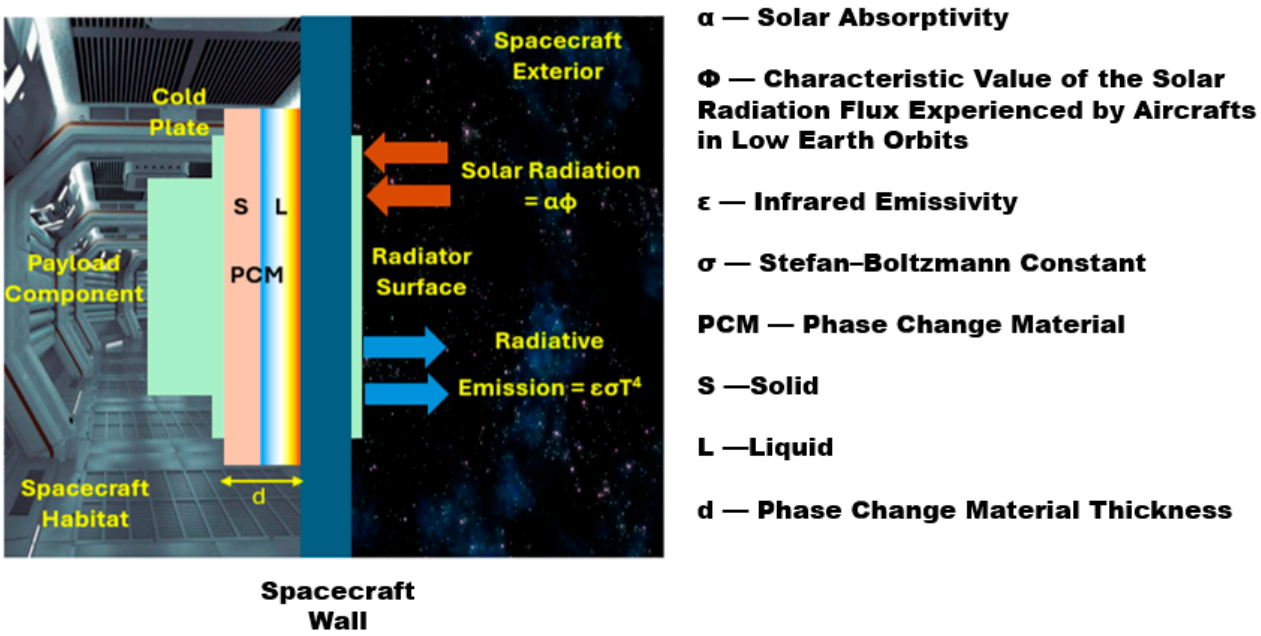

Figure 6. Scheme of the integration of a generic phase change material in a spacecraft radiator.

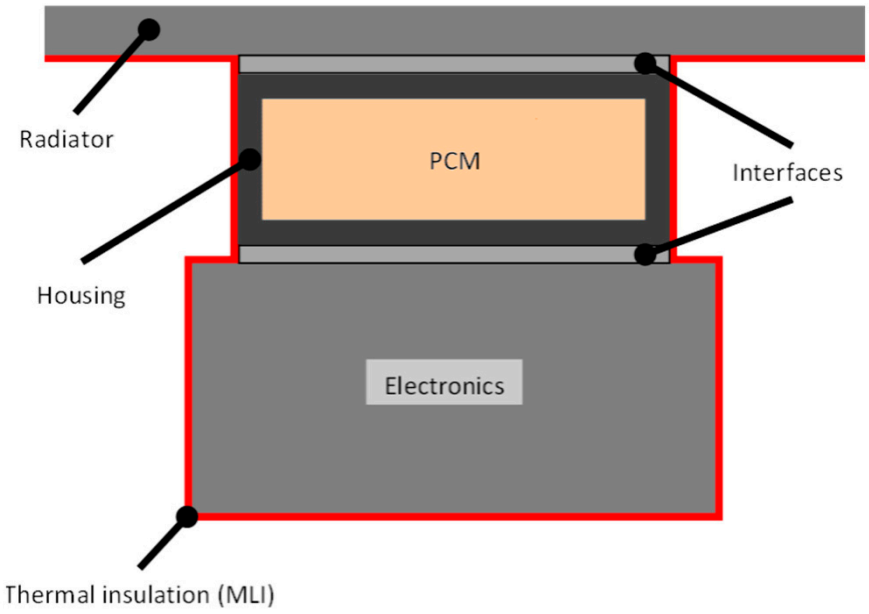

Figure 7. Scheme of the integration of a generic phase change material in the thermal management of electronics [52].

Moreover, it is also worth mentioning the synergistic effect of the addition of nanostructures like nanoparticles, nanowires, and nanotubes into phase change materials, forming the novel class of the nano-enhanced phase change materials. The incorporation will improve the thermophysical characteristics of the conventional phase change materials, especially paraffin waxes [53]. For example, researchers Khan and Khan et al. [54] added alumina, aluminum nitride, and graphene nanoplatelets into RT 44HC paraffin and used this solution in a shell and tube heat exchanger-based latent heat system. The nano-enhanced phase change material was poured into the shell of the heat exchanger. The authors confirmed that all types of tested nano-enhanced phase change materials enhanced the charging/discharging rates in comparison to those attained with pure paraffin. Also, the authors Krishna et al. [55] added alumina nanoparticles to tricosane phase change material for electronic cooling pur-

poses. The researchers used a heat pipe in which the phase change material was positioned at the adiabatic section of the pipe. The research team verified an around 25.8% reduction in the temperature at the evaporator when using the nano-enhanced phase change material. There were also reported to be more than 50% fan power savings in comparison with a conventional heat pipe. The nano-enhanced phase change material was also capable of storing approximately 30% of the energy supplied to the evaporator section.

2.3.3. Pool Boiling

Pool boiling is a heat transfer phenomenon characterized by the boiling of a pool of liquid on a submerged, heated surface. Cooling systems that utilize pool boiling have proven to be highly effective in dissipating heat due to the latent heat involved in the evaporation process and the fluid motion induced by the bubbles. The heat transfer coefficients (HTCs) of such systems are two orders of magnitude higher than single-phase heat transfer [56].

Pool boiling progresses through several stages connected to the wall superheat applied to the surface (the difference between the surface temperature and the saturation temperature of the liquid) [57]. The onset of boiling begins when the wall superheat is high enough to activate some of the nucleation sites (imperfections on the surface where evaporation tends to occur). This leads to a transition from convection heat transfer to the nucleate boiling regime. This heat transfer regime is characterized by a sudden increase in HTC, extracting high amounts of heat at low wall superheats. As the wall superheat increases further, more nucleation sites can be activated, increasing the mass of vapor covering the surface. As the density of sites increases, bubbles coalesce, forming larger vapor layers that cover and insulate the surface until it is completely covered in vapor.

This critical point is the critical heat flux (CHF), and it entails a drastic reduction in HTC and a sudden and dangerous increase in the temperature of the system. Thus, CHF is a vital limit in many boiling heat transfer applications, ranging from electronic cooling to nuclear reactor cooling and the thermal management of space stations and satellites.

During bubble growth and formation, several forces act on the bubble. The most relevant forces are the buoyancy force, dominated by gravity pushing the bubble away from the surface due to the difference in fluid density between the gas and liquid phases, and the surface tension force, dominated by surface characteristics such as wettability and roughness [58].

Space stations and satellites pose unique challenges as they operate in a microgravity environment, which affects the dynamics of nucleate boiling and CHF. If buoyancy is not acting on boiling, it is easier for bubbles to become stuck on the surface, quickly forming a vapor layer and decreasing the CHF. Therefore, gravity and surface characteristics need to be manipulated for these systems to function effectively in microgravity environments.

In this context, Garivalis et al. [59] conducted pool boiling experiments with FC-72 both on Earth and on board of a European Space Agency parabolic flight aircraft, which can suppress the effects of gravity. They evaluated highly wetting microstructured and plain heating surfaces, applying an external electric field to generate gravity-mimicking body forces. The results obtained revealed that microstructured enhanced surfaces increased the CHF in both terrestrial conditions and microgravity environments.

Furthermore, microgravity CHF enhancement on a plain surface can also be achieved by employing an external electric field. However, the best boiling performance is attained when these techniques are used together. The effects created by microstructured surfaces and electric fields are synergistic, enhancing the CHF in microgravity conditions up to 257 kW/m^2, a value even higher than that measured on Earth on a plain surface (168 kW/m^2).

Figure 8 presents experimental images of the pool boiling process under all tested conditions.

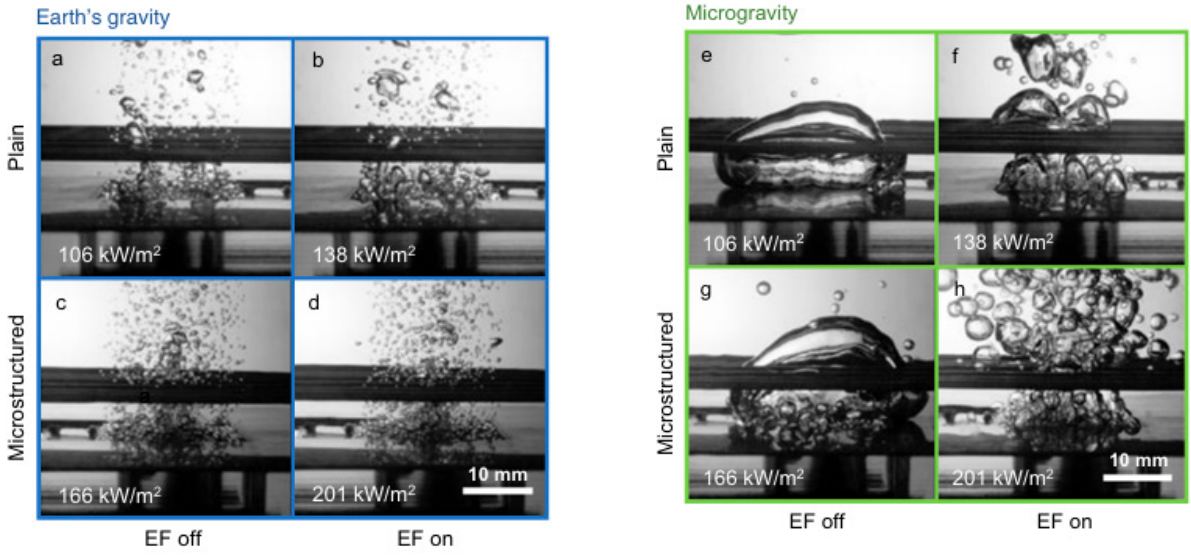

Figure 8. Experimental images of the pool boiling process in all the tested conditions: on Earth (**a**–**d**) and in microgravity scenario (**e**–**h**) on plain (**a**,**b**,**e**,**f**) and microstructured surfaces (**c**,**d**,**g**,**h**) with the application of an electric field and (**b**,**d**,**f**,**h**) without the presence of an electric field [59].

Additionally, Dhir et al. [60] conducted pool boiling experiments at the Boiling Experimental Facility located in the Microgravity Science Glovebox of the International Space Station. The BXF Facility was carried to the ISS on Space Shuttle Mission STS–133. The Nucleate Pool Boiling Experiment was one of the two experiments carried out in the BXF. The study covered single bubble dynamics (generation and growth), multiple bubble dynamics (lateral merger and detachment), nucleate pool boiling heat transfer, and CHF. FC-72 was used as the operating fluid, and the pressure system varied between 51 kPa and 243 kPa. The fluid temperature ranged from 30 °C to 59 °C, and the heating surface temperature varied from 40 °C to 80 °C. The heating surface was an aluminum disc with induced cylindrical cavities: four at the corners of a square and the rest in the middle. During the pool boiling experiments, the magnitude of gravity varied from 1.2×10^{-7} g to 6×10^{-7} g. The results showed that a single bubble continued to grow until it occupied the entire test chamber without detaching from the heating surface. During the lateral merger process of vapor bubbles, at high superheats, a large bubble may lift off from the surface but continue to hover nearby. Neighboring bubbles are continuously drawn into the large bubble. At low superheats, bubbles at neighboring sites simply merge to form a larger bubble. The larger bubble is mostly located in the middle of the heat transfer surface and serves as a vapor sink. This mode persists when boiling occurs all over the heating surface. Heat fluxes for nucleate boiling and CHFs were found to be much lower than those obtained under Earth gravity conditions.

So, the data are useful for calibrating numerical simulation results. Any correlations developed for nucleate boiling heat transfer under microgravity conditions must account for the existence of a vapor escape path from the surface, the size of the surface, and the size and geometry of the test chamber. Furthermore, verified heat fluxes for nucleate boiling were lower than prior results obtained on the space shuttle. The functional dependence of heat flux on wall superheat was found to be strongly dependent on pressure and liquid subcooling.

Additionally, the observed CHF, observed by the authors, was higher than that predicted by the hydrodynamic theory extrapolated to microgravity. Besides experimental conditions, the rate of nucleate boiling heat transfer will depend on the size of the heating surface and fluid confinement. Therefore, one should be extremely careful when extrapolating results from normal- and low-gravity experiments to microgravity conditions.

A critical issue in long-term space exploration is the storage and management of cryogenic propellants, given that storage tanks are exposed to very high temperatures and radiation. This exposure can create hot spots on the internal walls of the tanks, even with efficient temperature insulation. Counteracting the effects of heat sources on the propellant is crucial since bubbles may be generated, posing a danger to some engine components and reducing the amount of propellant.

Quintana-Buil and González-Cinca [61] conducted a study carried out in terrestrial gravity and in microgravity conditions on the effects of acoustic actuation on the heat transfer between a two-dimensional heating element and a liquid in a nucleate boiling regime. Two configurations of the heater orientation with respect to the direction of propagation of the acoustic wave and several acoustic frequencies were considered. Heater surface temperature and heat flux were measured in all the tests performed.

Acoustic actuation in microgravity increased the heat flux from the heater to the liquid by 8.6% in the terrestrial environment without actuation and 8.4% in the microgravity environment without actuation. The heat transfer enhancement was greater at frequencies with a higher acoustic amplitude and closer to the frequency of the piezoelectric acoustic actuator. The impact of the material of the heating surface on the acoustic field plays a relevant role in the heat flux and temperature tendencies.

The obtained results demonstrated that acoustic actuation is very suitable for the thermal management of boil-off in cryogenic propellants. The time evolution of the heating surface temperature and heat flux showed a ripple with the application of acoustic actuation, and the heater was on a substrate made of polymethyl methacrylate. This phenomenon may be linked to the fluctuating acoustic amplitude near the substrate. The acoustic field near the heating surface depends mainly on the acoustic impedance of the substrate material. When aluminum was employed, such amplitude fluctuations were not observed. Thus, for aluminum propellant tanks, a smoother trend of temperature and heat flux than in the experiments could be expected.

The decrease in temperature and the enhancement of heat flux when acoustic actuation is applied in microgravity should be explored to hinder bubble nucleation and therefore to control boil-off in propellant tanks. The diverse boiling features in the cryogenic propellants with respect to HFE-7100 would imply the use of distinct acoustic requirements. The main results demonstrate that the acoustic route is a very promising option for the thermal management of cryogenic propellants and electronics cooling operating in space conditions.

Moreover, Moehrle and Chung [62] conducted experimental tests in terrestrial and microgravity pool boiling using a platinum wire heater and FC-72 in the presence of an acoustic standing wave. The sound wave was created by driving a half-wavelength resonator at a frequency of 10.15 kHz. Microgravity conditions were produced by employing the 2.1 s drop tower on the campus of Washington State University. The burnout of the wire, commonly observed in heat flux-regulated systems, was avoided through a constant temperature controller to regulate the wire's temperature.

The amplitude of the acoustic standing wave was increased from 28 kPa to over 70 kPa, and these pressure measurements were made using a hydrophone fabricated with a piezoelectric ceramic. Cavitation incurred during experiments at higher acoustic amplitudes contributed to bubble dynamics and heat transfer performance. The wire was positioned at different locations within the acoustic field: the acoustic node, the anti-node, and halfway between these locations.

Boiling curves were obtained to show how the applied acoustic field improved nucleate boiling heat transfer performance and augmented the CHF in a terrestrial environment. Meanwhile, in microgravity, the acoustic field was found to be capable of filling the role of terrestrial gravity in maintaining the nucleate boiling heat transfer process.

Furthermore, the authors Zhang et al. [63] and Zhang et al. [64] investigated the nucleate boiling heat transfer of air-dissolved FC-72 on a micro-pin-finned boiling surface under microgravity using the drop tower facility in Beijing. The boiling surfaces, manufactured by dry etching, were composed of silicon chips with micro-pin fins with dimensions of

$30 \times 30 \times 60$ μm^3 (designated PF30-60) and $50 \times 50 \times 120$ μm^3 (designated PF50-120). The pool boiling process using a smooth surface was also studied in both terrestrial gravity and microgravity scenarios.

In general, the micro-pin fins showed better heat transfer capability than that attained using a smooth boiling surface under both Earth gravity and microgravity conditions. In the microgravity environment, this improvement was mainly due to the fact that the vapor bubbles generated on the micro-pin-finned boiling surface could depart from the heating surface in a continuous manner. For micro-pin fins, the reduced-gravity CHF was about two-thirds of that in the terrestrial environment experiment but almost three times as large as that for the smooth surface, which is larger than that in the Earth experiment. Under different gravity levels, the PF50-120 pins demonstrated a slightly better heat transfer performance than that of the PF30-60 pins, mainly because of the larger heat transfer area. Moreover, the fin gap of the PF30-60 pins could produce greater flow resistance for micro-convection near the fin side walls, resulting in a lower heat transfer performance.

3. Nanomaterials Applied in Aerospace Thermal Control

The utilization of nanomaterials offers the prospect of applying materials at the atomic and molecular levels, thereby advancing various properties relevant to engineering, including thermal conductivity, electrical conductivity, non-combustibility, mechanical strength, and optical characteristics [65]. This distinctive feature enables the integration of nanomaterials in aerospace applications, given the industry's demand for high-quality materials that deliver multifunctionality, reduced weight, extended service life, lower maintenance requirements, and enhanced reliability [66].

In this context, this chapter provides a summary of the application of nanomaterials in thermal control techniques. The types of nanoparticles employed, their implications, and key findings are addressed based on works published within the last three years.

3.1. Thermal Properties

The potential to modify the thermal properties of materials intended for space applications enhances the range of possible applications and has the potential to improve existing utilization conditions. For instance, an increase in thermal conductivity can facilitate the uniform dispersion of heat throughout the aircraft structure, preventing overheating and potential degradation, or even fire, in specific areas [7,67]. Conversely, it may also be desirable to employ materials with enhanced insulation capabilities to prevent substantial amounts of heat generated by hypersonic vehicles or atmospheric re-entry from reaching undesirable sections of the aircraft. Additionally, such materials can be utilized to prevent the loss of heat within survival cells [9,10]. Frequently, particularly in insulating materials, the objective is to elevate the onset temperature of material degradation, aiming to enhance safety and enable superior vehicle performance [10]. Here are some recent innovations for the utilization of these materials in the aerospace industry, particularly in polymer matrix composites and aerogels, which have been extensively explored in recent studies.

Epoxy is a widely used material in the structural components of the aerospace industry due to its ease of shaping, good mechanical properties, and thermal stability, despite having poor thermal and electrical properties. To address this issue, Hu et al. [67] employed carbon nanomaterials (CNTs) subjected to acid treatment before being mixed with graphene oxide in a molecular-level mixing process to obtain graphene oxide–carbon nanotubes nanostructures decorated with nickel nanoparticles (NiGNT). Seeking to enhance thermal and electrical conductivities, they utilized the magnetism of the particles to achieve nanostructured alignment in the vertical direction within the composite through the application of a magnetic field.

The results demonstrated that carbon nanomaterials interacted more effectively with the matrix than carbon fibers, yielding superior practical outcomes compared to theoretical calculations. The tested addition of up to 30% wt. showed a 2.7-fold increase in thermal conductivity in the direction where the nanoparticles were aligned. Additionally, there

was an improvement of approximately 10^4 in electric conductivity, accompanied by a decrease in the coefficient of thermal expansion from 13.45 µm/(m °C) in pure epoxy to 7.87 µm/(m °C) with the addition of nanoparticles [67]. Farzanehfar et al. [68] investigated a nanocomposite of epoxy with silica nanoparticles modified with sulfonic acid groups. The acid functionalization enabled the formation of new linkages, creating a core-corona structure. Subsequently, the nanoparticles were ionically tethered to a polymeric chain called Jeffamine-ED-2003, neutralizing the nanoparticles and allowing a network of connections that also ensured a certain distance between the nanoparticles. The results demonstrated not only high transparency (above 90%) and a slight increase in the material's degradation temperature but also highlighted these nanoparticles as high-performance additives, enhancing various properties such as bond strength, hardness, stiffness, crack propagation resistance, and shear strength.

Kaveh et al. [69] explored the utilization of SiO_2 (15–20 nm) and ZrO_2 (20–30 nm), whether functionalized or not, employing processes such as a vacuum furnace, ultrasonic bath, oil bath, and centrifugation. The functionalization was carried out using aminopropyltriethoxysilane, resulting in significantly improved mechanical outcomes with the functionalized nanoparticles. Furthermore, the functionalized nanoparticles also elevated the onset temperature of decomposition by 40 °C.

The thermoplastic poly(ether ether ketone) (PEEK) garners considerable attention in the aerospace industry due to its chemical resistance, capacity for fiber bonding, and high thermal stability, making it suitable for high-performance applications at elevated temperatures [70]. Hu et al. [67] combined carbon nanotubes (CNTs) and graphene oxide (GO) through molecular-level mixing with silver to form AgGNT nanostructures. The final composite featured AgGNT at a weight percentage of 30%, resulting in a 90% improvement in thermal conductivity compared to the matrix material, along with a 109-fold enhancement in electrical conductivity. The material also exhibited increased resistance to temperature and pressure, showing no significant alterations in its nanostructure even when subjected to a temperature of 400 °C and a pressure of 103 Pa.

Islam et al. [71] incorporated SiC nanoparticles (cubic form, 40 nm) and TiO_2 nanoparticles into an epoxy and Kevlar 29 composite. The nanoparticles were mixed with epoxy and hardener before the resin was used in the dip-coating process. The Kevlar fibers underwent cutting, cleaning, and thermal treatment before being combined with the resin containing nanoparticles. The result was a composite with improved thermal stability due to the adherence of nanoparticles to the fibers through molecular adhesion. The glass transition temperature rose from 559.13 °C to 580.51 °C.

Wang et al. [9] incorporated graphene platelets, carbon nanotubes (with diameters of 8–15 nm and lengths approximately 50 µm), and boron nitride nanosheets (with a hexagonal crystal structure of 30–50 nm) into an epoxy matrix. The particles were washed with acetone and underwent an ultrasonication process, followed by stirring with epoxy and subsequent degassing. The addition of nanoparticles led to a significant improvement in thermal conductivity, reaching close to 0.8 W/(m K), which was 400% higher when using carbon nanotubes. With the addition of graphene platelets, it approached approximately 0.5 W/(m K), along with enhanced mechanical properties, particularly in adhesive strength, as depicted in Figure 9.

Leow et al. [8] investigated a PEEK matrix with carbon fiber for applications in electrostatic dissipation, heat regulation, and lightning strike protection. Graphene nanoparticles were introduced through spray deposition, employing an aqueous solution with 2% wt of graphene, within the layers of the composite material to functionalize the carbon fibers. The addition resulted in a remarkable 252% improvement in thermal conductivity in the transverse fiber direction, enhancing the thermal diffusivity by up to 183% in one direction, with an optimal addition of 0.7% wt. Figure 10 illustrates insightful graphs depicting these enhancements. However, shear strength decreased with the incorporation of graphene, likely attributed to an increase in void volume due to surfactant vaporization during thermal treatment.

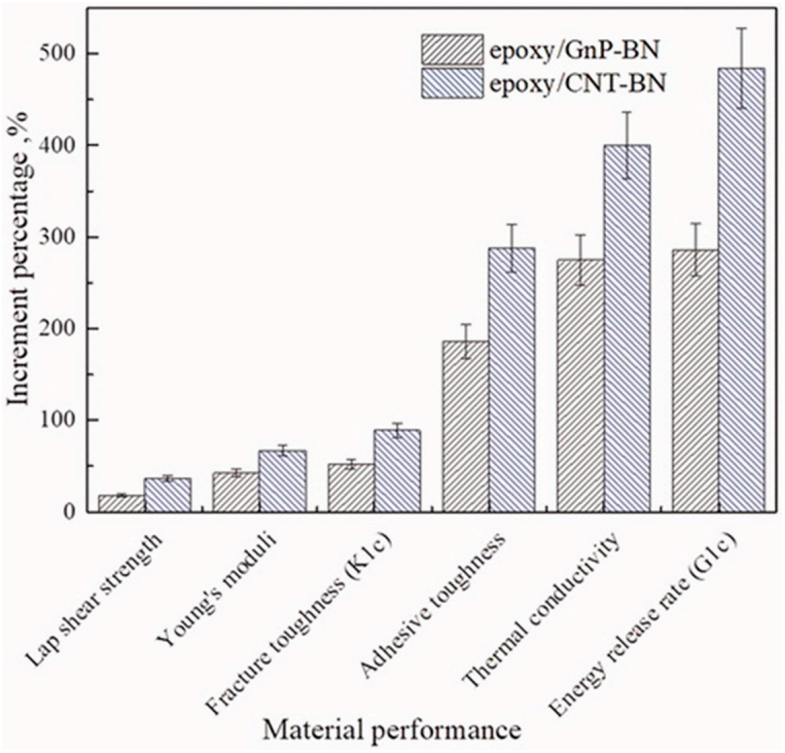

Figure 9. Enhancement of epoxy resin properties through the addition of GNP-BN or CNT-BN nanoparticles. Obtained from Wang et al. 2021 [9].

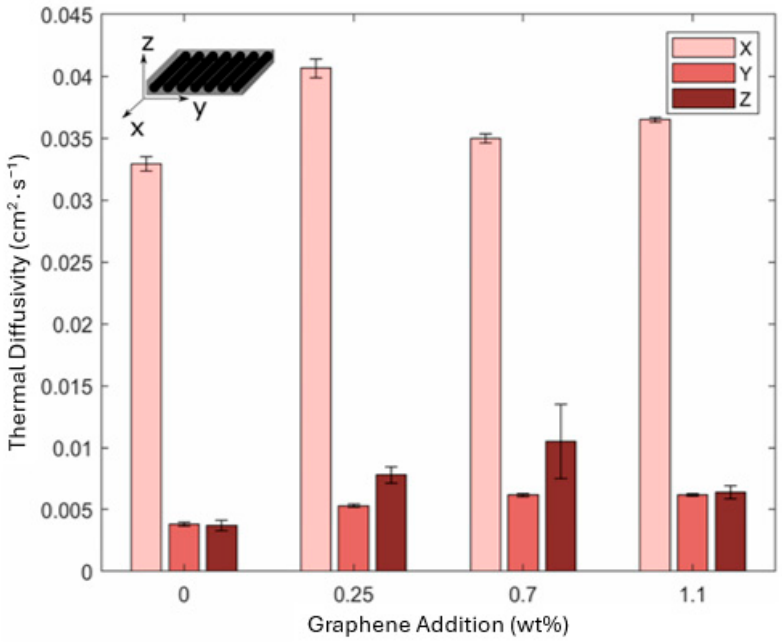

Figure 10. Thermal diffusivity in a PEEK matrix nanocomposite with carbon fibers and graphene addition in different directions as a function of the percentage of added graphene. Obtained from [8].

Thermosetting composites have been extensively utilized in the aerospace industry, but their use requires caution due to the release of toxic gases when exposed to fire. The utilization of biocomposites can mitigate this issue. In this context, Azad et al. [72] incorporated silica nanoparticles to retard flame formation and spread within a jute/thermoplastic starch (TPS) matrix. The addition of these nanoparticles can also positively influence mechanical properties by enhancing tensile, flexural, and impact resistance properties [73].

3.2. Thermal Control Coatings

Thermal control coatings (TCCs) play a crucial role in the realm of aerospace objects, serving as a vital tool for maintaining temperatures within a safe range for internal instruments and payloads. These coatings are instrumental in preventing external heat sources from causing undesirable temperature increases. Heat transfer occurs through radiation, with solar radiation, albedo radiation, and planetary radiation constituting the primary sources. Additionally, internal components such as instruments, cameras, and microprocessors contribute to heat generation, necessitating efficient heat dissipation through radiation. Consequently, an ideal TCC should not only prevent excessive heat input but also facilitate the removal of internally generated excess heat [74].

A high-quality TCC must possess suitable absorption and emissivity parameters, coupled with excellent thermal stability, strong adherence to the aerospace object's structure, appropriate mechanical properties, and corrosion protection [74,75]. Achieving these parameters often involves incorporating features such as adequate roughness, a multiphase and multi-component structure with significant thickness, and a porous surface structure [74].

Polyurethane coatings are utilized on the surfaces of aerospace objects due to their favorable balance between mechanical and chemical properties. In the pursuit of enhancing the curing processes for polyurethane coatings and employing more environmentally friendly solvents, Zareanshahraki et al. [76] developed aerospace UV-curable coatings based on NIPU acrylate. The radiation cure technology presents advancements such as lower energy requirements, the avoidance of volatile organic compound emissions, reduced space requirements, and the ability to facilitate rapid polymer network formation. The results indicated that the developed coating exhibits commendable flexibility at low temperatures and substantial resistance to specific chemical products.

In the study conducted by Chen et al. [77], a paint applicable through spray, dipping, or brushing demonstrated an infrared emissivity exceeding 0.95 and a solar radiation reflection capacity approaching 90%. Formulated from a solution of aluminum phosphate and metakaolinite, this paint is categorized as an all-inorganic phosphoric acid-based geopolymer. Notably, it possesses the advantage of being less susceptible to space irradiation and high temperatures compared to organic polymers. The results also showcase its robust performance against mechanical stress, affirming its suitability for application on aerospace objects.

Spacecraft face extreme temperature gradients, which can affect the efficiency and lifespan of onboard systems. As a result, thermal control coatings (TCCs) are used to maintain the spacecraft components at an operational temperature to ensure optimal performance by reflecting solar radiation and emitting internal heat [78]. Considering their optical characteristics, the thermal control coatings can be categorized into four primary classifications: (i) solar absorbers, (ii) solar reflectors, (iii) flat absorbers, and (iv) flat reflectors [78].

A reflective TCC consists of materials applied to spacecraft that are able to reflect solar radiation and minimize heat absorption. Due to their inherent reflective properties, zinc oxide powders are commonly used as pigments for reflective TCCs. However, the conventionally used zinc oxide powders are not able to maintain their function efficiently in longer missions (15 to 20 years). Mikhailov et al. [79] studied the influence of the addition of SiO_2 nanoparticles on the solar absorption (αs) of a thermal control coating (TCC) to improve the radiation resistance and longevity of TCCs. The coating under study consisted of zinc oxide pigments and lithium silicate binder, to which the authors added 3% wt. and 0.5% wt. of SiO_2, respectively, to enhance their resistance to electron irradiation. Changes in αs and how this was influenced by electron irradiation in the presence of SiO_2 nanoparticles were studied. The modified TCC (TCCmod) was found to increase the resistance of TCCs to electron irradiation compared to the unmodified TCC (TCCunmod). For this, the αs variation ($\Delta\alpha s$) between the two coatings was estimated for geostationary orbit (30 keV electrons and F > 7.1016 cm^{-2}) by electron exposure for the periods of 5, 10, 15, and

20 years. The $\Delta\alpha s$ between TCCmod and TCCunmod increased, revealing values of 1.54, 1.74, 1.88, and 1.95 for the corresponding periods. These results demonstrate the potential for altering pigments and binders by adding nanoparticles to improve radiation resistance in outer space.

Also, nanomaterials like zinc oxide quantum dots (ZnO QDs) demonstrate enhanced reflectance in the ultraviolet (UV) to near-infrared (NIR) spectrum as a result of quantum confinement and scattering effects [5]. The choice of ZnO results from the low solar absorbance demonstrated by this compound (minimizing heat absorption) and radiation resistance (ideal for long-term space applications) [6]. However, it is imperative to apply passivation to the ZnO QDs to ensure a more stable emission of exciton UV to prevent their aggregation and surface recombination. Consequently, silicon dioxide as a passivation material has been shown to enhance reflectivity in the NIR range. Chen et al. [80] presented a straightforward approach to creating ZnO QDs/SiO_2 composite pigments using the rapid injection sol–gel method. The sintering temperature was optimized to adjust the ZnO QDs size, which led to a high reflectivity in the UV/VIS region obtained by sintering at 300–500 °C. The proposed composite pigment achieved a reflectance above 60% in the full solar spectrum (200–2600 nm). Furthermore, Delfini et al. [74] proposed an innovative concept of TPS for reusable launch vehicles (RLVs) based on the coating of carbon/carbon substrates using pyro-paint ceramic varnish charged with silicon oxide nanoparticles (1% wt.) due to their ability to lower the thermal conductivity of materials. Based on the coefficient of thermal expansion (CTE), the authors demonstrated the improved stability of the nanoparticle-filled coating at high temperatures (up to 1400 °C) compared to the basic coating. Furthermore, the substrate coated with varnish-enriched NPs showed a decreased thermal conductivity of about 4–7%.

Nanoparticle-based coatings have also been investigated to improve radiative cooling systems. This type of system performs passive cooling in response to the temperature difference between the Earth (~300 K) and outer space (~3 K) [81,82]. These systems are especially interesting for reducing energy consumption and its inherent benefits. Alimohammadian and Dinarvand [83] proposed a coating based on a double-layer nanoparticle layer and a ballistic thermal rectifier to improve the efficiency of a common thermal radiative cooler. The proposed idea aimed to inhibit heat distribution by keeping the face exposed to solar energy away from the body, leading to decreased body temperature and a higher operating temperature for the emitter section. For this, the authors explored a structure constituted by (i) an emitter layer composed of silica, (ii) a reflector layer composed of titanium dioxide nanoparticles (TiO_2), and (iii) a ballistic thermal diode. The titania layer was composed of nanoparticles with sizes of 200 nm since this size is the most suitable for formulating a layer with the highest reflectivity. Furthermore, the thermal diode allowed the object's surface to continue radiating heat, further enhancing the cooling performance. The results demonstrate the efficiency of the proposed strategy in terms of efficient cooling rates, high resistance to thermal shock, and superior performance in cloudy weather conditions.

Plasma-spraying technology is used to deposit various materials (polymers, metals, composites, and ceramics, among others) on aerospace structures [84]. This technique forms a thick protective coating and promptly has the most significant advantage of a high deposition rate [85]. Furthermore, this type of coating is associated with increased chemical, thermal, and corrosion resistance [86]. Alumina-based coatings are highly used in the aerospace industry due to their weight ratio properties, high thermal conductivity, and good corrosion resistance [87]. Although they have clear advantages, they have poor strength at elevated temperatures and a susceptibility to stress corrosion cracking (SCC). These limitations of thermal and mechanical properties can be counteracted by adding micro- or nanomaterials to aluminum alloys or optimizing the coating process. He et al. [88] explored the mechanical and thermal properties' differences between conventional (CC) and nanostructured (NC) alumina coatings prepared using plasma-spray technology. The NC revealed a higher hardness value (1168.8 HV) and a reduced solar absorbance (0.26) compared to the CC (1079.7 HV and 0.324, respectively) within the 200–2500 nm wavelength

range (Figure 11) [88]. As expected, the distinct microscopic morphology between the two types of coating is responsible for differences in spectral reflectance. Plasma-sprayed nano-alumina coatings are commonly heterogeneous and often characterized by a porous microstructure. When radiation enters the coating, volume scattering occurs due to the differences in optical indices between the air within the pores and the matrix. This leads to a modified radiation direction and multiple reflections between the heterogeneity and matrix at the interface. Consequently, there is a contribution to the reflectivity of the coating.

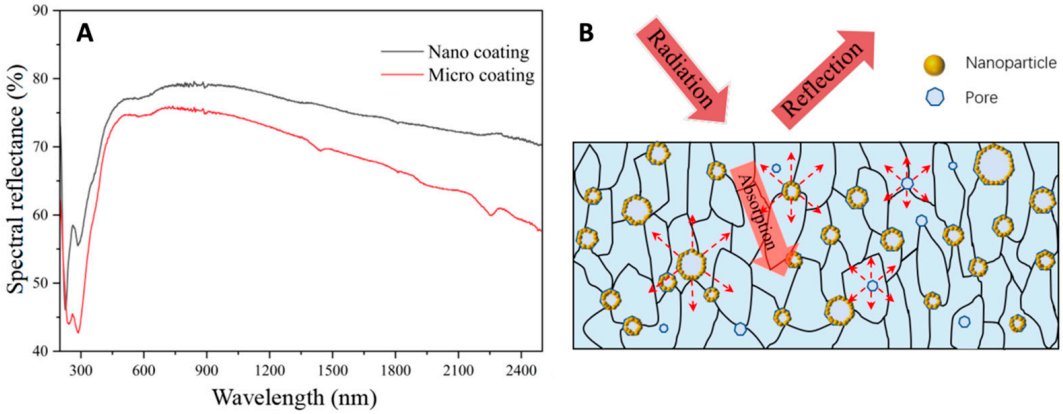

Figure 11. (**A**) Spectral reflectance (%) of conventional (micro coating) and nanostructured (nano coating) Al_2O_3 coatings within the wavelength range of 200 nm to 2500 nm. (**B**) Schematic representation of the radiation on nano-alumina coatings produced by plasma spraying. Adapted from [88].

3.3. Thermal Protection Materials

Thermal protection system (TPS) materials are vital in the aerospace industry by acting as a heating shield on aerospace structures during atmospheric entry or propulsion. Aerospace materials are subject to extreme conditions, such as high thermal variations, different chemical environments, and high mechanical stress [89]. They are fundamental to protecting the aerodynamic surfaces, the payloads and the vehicle's structure from hyperthermal environments [90]. Based on their working principles, TPs materials can be distinguished as (i) non-ablative TPS, which rely on re-radiation to insulate (using, for instance, tungsten and rhenium or ceramics), or (ii) ablative TPS, which use ablation to dissipate heat (usually using polymers) (Figure 12) [91,92]. Considering the limitations of conventional materials, composite materials have been preferred for structural elements and thermal protection. Composite materials are classified according to the matrix material and type of reinforcement and include, for example, ceramic matrix composites, metal matrix composites, and polymer matrix composites [93].

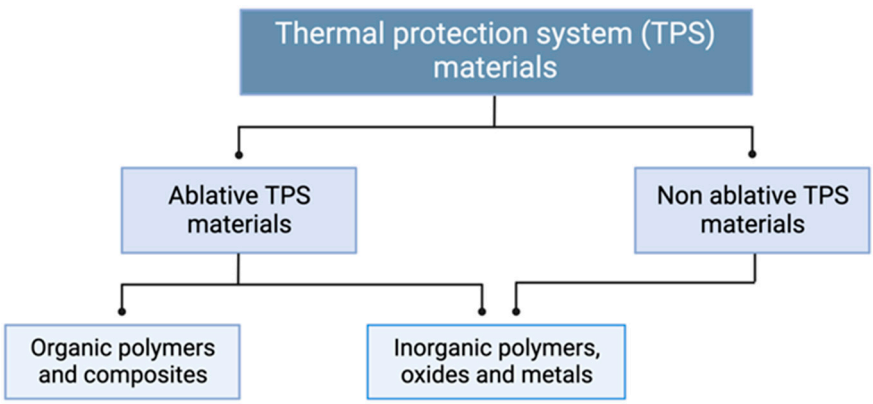

Figure 12. Classification of thermal protection system materials.

Nanocomposites containing carbonaceous fillers can augment the mechanical and electrical characteristics of aerospace materials, greatly contributing to diminished aerospace weight and overall costs and emissions [94]. Carbon nanotubes (CNTs), graphene, and carbon nanofillers (CNFs) are among the most widely studied and applied carbonaceous fillers. Using this carbonaceous type offers multifunctionality to the composites since, for example, CNTs have excellent mechanical and electrical properties, CNFs have a large aspect ratio, and graphene has a high surface area [95]. However, the usual methodologies used to incorporate carbonaceous fillers in polymer matrices present some limitations, like, for instance, their aggregation or bad dispersion. In turn, the CNF or CNT aggregation decreases the nanocomposite's mechanical properties by weakening the polymer–nanofiller interfaces. As a result, Öztürkmen et al. [96] proposed three-roll milling to enhance the dispersion and distribution of GNT and CNT into high-temperature curing resins. The three-roll milling integrated the carbonaceous fillers into the epoxy matrix with high homogeneity, enhancing the filler dispersions. Furthermore, the results demonstrated that the electrical conductivity of the nanocomposites can be tailored without affecting their mechanical or physical properties.

Also, carbon–phenolic composites are essential for the thermal protection of space vehicles due to their exceptional ablative performance [97]. These composite materials demonstrate exceptional resistance to ablation when subjected to high-temperature environments such as oxyacetylene flame and plasma wind tunnels. The incorporation of carbon-based and ceramic additives into carbon–phenolic systems has the potential to enhance their density and ablative, thermal, and mechanical characteristics. Ahmad et al. [98] conducted a comparative study that explored advancements in the literature regarding ablative composites, specifically carbon–phenolic composites, for enhanced aerospace applications. In their research, they compared the effects of different carbon-based and ceramic additives on the properties of fiber-reinforced polymer matrix composites. The goal was to establish a relationship between the structure and properties by investigating how various filler systems affect the ablation mechanism. The authors' main findings showed that (i) the inclusion of silicon dioxide (SiO_2) nanoparticles allow for an increase in ablation resistance by creating a carbon–silicon carbide layer that can withstand high temperatures and shear forces; (ii) high concentrations of fillers such as nano-SiO_2 may result in reduced interlaminar shear strength due to poor adhesion; (iii) ceramic particles like zirconium carbide (ZrC) and silicon carbide (SiC), at optimal concentrations, can decrease ablation rates but may increase them if the concentrations are too high; (iv) the addition of zirconium silicide ($ZrSi_2$) additives significantly reduces mass ablation rates by forming a protective layer consisting of SiO_2 and zirconia (ZrO_2); and (v) carbon nanotubes enhance mechanical properties and decrease the ablation rate, but they also increase thermal conductivity [98].

Lightweight ablators are low-density and weight-bearing ablators capable of withstanding extreme heat [99]. They are composed of materials like carbon fiber reinforcement and porous phenolic resin matrices [100], but most of the conventional ablators lack oxidation–ablation resistance when exposed to extreme thermal environments. Considering the need for lightweight ablators with high compressive strength and great elasticity for thermal protection, Jin et al. [101] developed a novel needle carbon fiber-enhanced siliconoxycarbide–phenolic-interpenetrating aerogel (SiCF/PR) nanocomposite. Compared to the conventional ablators, the SiCF/PR nanocomposite demonstrated enhanced oxidation and ablation resistance, withstanding a 1000 °C flame for 30 min without structural disintegration. Furthermore, it demonstrated a higher compressive strength (4.57 to 5.83 MPa), superior thermal insulation (thermal conductivity of 0.068 W/(m·K)), great elasticity (7.35 MPa), and durability (it maintains 81% of the maximum stress and 76% of modulus after 100 cycles).

In the work by Wang et al. [11], the authors drew inspiration from the insulation properties of polar bear fur to create an aerogel with TiO_2 nanorods. The concept involved using these nanorods as an interfacial reinforcement phase between hollow mullite fibers and the aerogel. The nanorods were generated on the surface of the hollow mullite fibers

through the hydrothermal method. The results demonstrated that the material maintained its insulating properties with a thermal conductivity of 0.041 W/(m K) and improved infrared transmittance, reaching approximately 0% at a temperature of 1200 °C [11].

Kong et al. [10] employed surfactants to disperse dry aerogel particles and hydroxyapatite (HAP) nanowires in an aqueous solution, yielding aerogels that, combined with reflective screens, formed a multilayered material capable of withstanding temperatures up to 1000 °C. The resulting material exhibited excellent insulation properties, with a thermal conductivity of 0.028 W/(m·K) at room temperature and 0.059 W/(m·K) at 800 °C [10].

Furthermore, the introduction of yttrium oxide (Y_2O_3) nanoparticles and chromium nanoparticles can enhance the high-temperature properties of cooper–chromium (Cu-Cr) alloys [102]. Cu-Cr alloys are important materials for aerospace applications since they combine high strength and thermal conductivity. Y_2O_3 nanoparticles pin dislocations and grain boundaries, enhancing high-temperature tensile strength and softening resistance, while chromium nanoparticles inhibit the growth of Cr particles, contributing to the alloy's high-temperature stability. As a result, the thermal conductivity of the ODS Cu-Cr-Y alloy increases to 243 W/(m·K) at 600 °C, exhibiting superior high-temperature tensile strength and softening resistance compared to traditional Cu-Cr alloys.

Nanomaterials can also be utilized to develop pressure sensors that can function effectively even at high temperatures. Wang et al. [103] presented a technique in which SiO_2-encapsulated Ag nanoparticles were attached to SiO_2 nanofibers. This approach aimed at augmenting both the stability and performance of the sensors. The decision to use Ag nanoparticles was to ensure conductivity in the nanofiber membrane, which is otherwise insulating. Additionally, the Ag coating with SiO_2 was applied to prevent migration and fusion, thus improving thermal stability. The outcome of this research showcased pressure sensors with exceptional sensitivity. Moreover, these sensors were able to operate consistently at temperatures as high as 350 °C, and their performance remained intact even after being subjected to annealing at 600 °C for a duration of 2 h.

Molybdenum disulfide (MoS_2) is an efficient electrocatalyst used as an alternative to platinum catalysts for H_2 evolution reactions (HERs). Those properties are leveraged in energy conversion and storage systems, such as lithium batteries, which are integral to aerospace power systems. Furthermore, they act as a solid lubricant in satellites due to their excellent tribological properties. However, the exposure to high-temperatures induces the oxidation of MoS_2, affecting its mechanical stability and surface chemistry. Rahman et al. [104] conducted a study on the high-temperature oxidation of monolayer MoS_2 and its impact on mechanical properties using ReaxFF molecular dynamics simulations. The oxidation kinetics of MoS_2 at elevated temperatures (1400 K, 1500 K, and 1800 K) revealed that MoS_2 readily reacts with O_2 above 1500 K. Also, the mechanical properties were found to degrade significantly upon oxidation. The pristine MoS_2 monolayer exhibited a fracture stress and strain of 24 GPa and 27, respectively, while the oxidized sample showed reduced values of 16 GPa and 25.5. Understanding the impact of elevated temperatures on the oxidation processes of MoS_2 (or another type of material) and its effects on mechanical and chemical properties is crucial in this field of study.

Another type of nanomaterial pointed to enhance the thermal protection capabilities of materials used in aerospace applications includes preceramic polymer-grafted nanoparticles (PCP GNPs). The integration of PCP GNPs into ceramic matrix composites (CMCs) can improve the thermal stability of these materials. However, there is a lack of understanding about the material transformations during low-temperature thermal treatment prior to pyrolysis. In a study conducted by Martin et al. [105], two different types of PCP GNPs (poly(1,1-dimethylpropylsilane) (allyl-GNP) and poly(1,1-dimethylbenzylethylsilane) (styryl-GNP)) were subjected to thermal treatment at temperatures up to 250 °C prior to pyrolysis. When undergoing the low-temperature thermal treatment, both exhibited an increased char yield at 800 °C, which is a desirable property for thermal protection. The styryl-GNPs in particular showed a curing event between 180 °C and 250 °C, which led to the formation of a network structure contributing to the improvement in char yield. This

is associated with a transition from diffuse to ballistic behavior. Furthermore, the storage modulus revealed unique moduli changes for each material. Overall, the result suggests that the chemical structure of the grafted polycarbosilane chains plays a significant role in the thermally induced changes to the structure and behavior of the PCP GNPs.

4. Nanofluids

The ever-increasing miniaturization of the thermal management systems fits very well with the reduced space and weight and energy constraints existing in the International Space Station and space aircraft. In this scenario, the novel class of thermal fluids recognized by nanofluids with superior thermophysical properties is capable of providing the cooling and heating rates of very high imposed heat fluxes. The enhanced heat transfer characteristics of the nanofluids make them very promising alternatives to simplify and miniaturize the heat transport equipment and systems on spacecrafts [106]. Apart from the heat transfer capability, the nanofluids operating in microgravity conditions will mitigate or even eliminate the limitations linked with stability in time aggregation and sedimentation, which troubles investigators in terrestrial environments.

Das [106] proposed the exploration of nanofluids in ATCSs (active thermal control systems) to cool electronic equipment and environments. Ungar and Erickson [18] carried out a parametric study to address the employment of nanofluids in spacecraft ATCSs. The authors concluded that the inclusion of nanoparticles in the traditional spacecraft thermal base fluids could decrease the size, mass, and pumping power requirements of the thermal management systems.

Additionally, the researchers Kuo et al. [107] confirmed that the solid fuels containing a considerable percentage of nanoparticles are remarkably beneficial. The obtained results indicated that at a moderate mass flow rate, the solid HTPB (hydroxyl-terminated polybutadiene) fuel containing 13% of aluminum powder exhibited a 123% greater linear regression rate than that attained with the non-aluminized HTPB fuel. Therefore, the authors concluded that the addition of nanoparticles increased the heat transfer capability and the specific energy release of rocket propellants.

In the numerical simulation field, the recent study conducted by Yanaoka and Inafune [108], who performed numerical simulations of the natural convection of nanofluids between plates in microgravity with gravity modulation, can be highlighted. The Rayleigh number was 3×10^6, and the dimensionless frequency of the gravity modulation F varied up to 10^2 at volumetric concentrations up to 0.05% vol. The researchers investigated the variation in time of thermal convection structures under gravity modulation and the frequency response of the heat transfer characteristics to the gravity modulation. For a concentration of 0.01% vol., the fluid followed the low-frequency gravity modulation of F = 1 well. Therefore, the thermal convection repeatedly developed and decayed as the gravity acceleration increased and decreased. At a high-frequency gravity modulation of $F = 10^2$, since the flowability of the fluid was poor, the convection remained during one cycle of gravity modulation. At a frequency equal to one and at 0.01% vol., the Nusselt number was between 1 and 1.1 times greater than that attained without the inclusion of nanoparticles over one period.

Also, it was confirmed that the HTC (heat transfer coefficient) was lower at low frequencies than at high frequencies, regardless of the concentration of the nanoparticles. At 0.01% vol., the average Nusselt numbers for frequencies equal to one and five were between 1 and 1.01 times greater than the one achieved without the addition of nanoparticles, and the reduction in the HTC owing to the nanoparticles was suppressed. At 0.05% vol., for each frequency, the Nusselt number was much lower than the one without the incorporation of nanoparticles. Consequently, for low-frequency gravity modulations that make damping difficult, employing nanofluids with a volumetric concentration of 0.01% vol. can prevent the HTC deterioration.

Mohamed et al. [109] conducted an experimental and numerical investigation on the behavior of a flow-boiling nanofluid within a rectangular channel. The nanofluid, comprising a salt solution (acetone/$ZnBr_2$) as the base matrix, incorporated graphene nanoparticles at varying volumes (0.1%, 0.2%, 0.3%, 0.4%, and 0.5%). The experimental setup involved a 250 W heater located at the boiler section, controlled by a PID system, to heat a flow rate of 3.63 cm^3/s. The results revealed that an increase in nanoparticle volume led to a reduction in pressure, decreasing from 1.3 bar to 1.24 bar as the volume concentration increased from 0.1% to 0.4%. This phenomenon is attributed to the exponential rise in thermal conductivity, enabling enhanced heat transfer to the fluid.

Additionally, this increase in nanoparticle concentration had repercussions on the saturation temperature of acetone, which rose due to pressure differences. Computational fluid dynamics (CFD) utilizing the volume of fluid (VOF) method yielded better agreement with heat flux and the heat transfer coefficient than temperature measurements. The simulation illustrated that evaporation led to an increase in salt concentration, resulting in less liquid contacting the hot surface and reducing bubble formation.

In turn, Chen et al. [110] conducted an experimental investigation utilizing a pool boiling system within a centrifugal acceleration machine capable of achieving 3 g hypergravity. The pool boiling section featured a platinum wire with a diameter of 50 μm, and the nanofluid employed was based on water with Al_2O_3 nanoparticles (ranging from 0.001 wt% to 0.015 wt%) dispersed with the assistance of dispersant sodium dodecyl benzene sulfonate (SDBS). The results demonstrated that the use of the dispersant led to a decrease in the CHF, while an increase in pressure contributed to an enhancement in the heat flux. Furthermore, the findings indicated that the introduction of nanoparticles increased the CHF up to 2 g gravity, after which this parameter began to decline, possibly due to the substantial deposition of nanoparticles. The presence of nanoparticle coatings on the tube walls influenced wettability, creating a porous surface and increasing bubble nucleation points, consequently elevating the heat flux, despite a simultaneous increase in local temperature.

Arif et al. [111] studied the enhancement of a radiator's thermal conductivity and heat transfer performance using water-based ternary hybrid nanofluid with differently shaped nanoparticles. For this, the authors employed a fractional model to analyze the heat transfer, considering nanoparticle shape factor and sphericity. The researchers considered a combination of spherical-shaped aluminum oxide (Al_2O_3), cylindrical carbon nanotubes (CNTs), and platelet-shaped graphene nanoparticles suspended in a single base fluid to form the hybrid nanofluid. The thermal performance of this ternary hybrid nanofluid was superior to that of unitary nanofluids, enhancing the heat transfer rate by up to 33.67%. This enhancement is attributed to the increased surface area and improved thermal interactions at the nanoparticle–fluid interface due to the shape factor. The fractional model developed in this work is fundamental to predicting the thermal behavior of nanofluids, facilitating the design process to achieve more efficient heat exchange systems. In turn, Henein et al. [112] investigated the thermal performance of an evacuated tube solar collector (ETSC) using a hybrid nanofluid composed of magnesium oxide and multi-walled carbon nanotubes (MgO/MWCNT) in various weight ratios. MgO/MWCNT hybrid nanofluids demonstrated optimal thermal efficiency at a 0.02% nanoparticle concentration.

Furthermore, varied volume flow rates (1–3 L/min) and MgO/MWCNT weight ratios (80:20 to 50:50) were tested, and it was concluded that higher MWCNT ratios and flow rates enhanced thermal performance. The 50:50 MgO/MWCNT hybrid nanofluid demonstrated the highest thermal performance compared to the other hybrid nanofluids. Specifically, its energy efficiency enhancement was found to be 55.83%. The overall results suggest that the synergistic effect of combining MgO and MWCNT nanoparticles at a 50:50 weight ratio in a water base is highly effective for improving the energy efficiency of ETSCs.

Apart from the mentioned studies, other ones are referred in different sections of the current review, including flow and pool boiling and heat pipes. Table 1 summarizes some of the recently available works on the use of nanofluids in aerospace applications, with emphasis on the chemical composition, concentration, and main findings related to the nanofluids.

Table 1. Main findings related to the use of nanofluids in aerospace applications.

Authors	Nanoparticles	Base Fluid	Concentration	Main Findings	Reference
Wu and Kumar	Alumina	Water	1–5% vol.	The HTC and Nusselt number increased for all concentrations in comparison to those of water alone. The HTC at the maximum concentration was 9.1% and 9.7% higher than those of the water for expansion ratios of 1.9 and 3.5, respectively. The coefficient of skin friction and outlet temperature decreased for all concentrations.	[113]
Chen et al.	Graphene	Silicone oil	Up to 10% vol.	The thermal conductivity of the nanofluids increased with the growing concentration of graphene. Under these conditions, the temperature gradients at the two ends of the cavity decreased gradually, and the temperature gradient in the middle of the cavity augmented. In comparison with pure silicone oil, the Nusselt number of the graphene/silicone oil nanofluids with concentrations of 1, 2, 3, 4, 6, 8, and 10 vol.% decreased by 42.1%, 61.8%, 69.7%, 78.9%, 88.1%, 86.8%, and 92.1%, respectively.	[114]
Zhang et al.	Copper	Water	---	The increasing strength of frequency of oscillation and incline angle led to reductions in the skin friction coefficient and HTC, but an opposite trend was found when the thermal buoyancy was enhanced. The increasing radius of the nanoparticles and frequency of oscillation led to a decrease in the skin friction and HTC, but an opposite trend was reported for the Nusselt number against the increasing radius.	[115]
Dong et al.	Alumina	Water	0.07–0.1% vol.	The boiling HTC increased with increasing mass flow rates but decreased with an increase in the aspect ratio of the microchannels under terrestrial gravity and acceleration fields. The HTC under acceleration conditions was slightly smaller than that under terrestrial gravity. The HTC increased with increasing the concentration of nanoparticles for values up to 0.075 vol., but it decreased as the concentration increased from 0.07 vol.% to 0.1 vol.%. The impact of the acceleration magnitude and direction on the boiling heat transfer was noticeable. The HTC was reduced with increasing acceleration magnitudes.	[116]

Table 1. *Cont.*

Authors	Nanoparticles	Base Fluid	Concentration	Main Findings	Reference
Wu et al.	Platinum capped with hydrophobic hyperbranched polyglycerol	Methylcyclo-hexane	23–33% wt.	The nanofluids were stable after a 180-day storage period. On a simulated cooling channel of aircraft, the cracking performance and the energy absorption capacity when using the nanofluids were promoted significantly. At 650 °C, the heat sink reached 2.39 MJ/kg with an increase of 20.7% in comparison to thermal cracking. Larger macroinitiators with hydrophobic hyperbranched polyglycerol were beneficial since to acquire the same heat sink of 2.20 MJ/kg, the temperature can be reduced from 675 °C to 664 °C, 653 °C, and 638 °C for the macroinitiators with molecular weights of 3 k, 5 k, and 13 k, respectively.	[117]
Hussain	Copper and copper and graphene oxide	Sodium alginate	---	The copper–graphene oxide/sodium alginate hybrid nanofluid had higher thermal conductivity than that of the copper/sodium alginate nanofluid. The heat transfer rate increased with the growing concentration of nanoparticles. The entropy of the system was enhanced with increasing material factor, Reynolds number, thermal radiation factor, and concentration of nanoparticles.	[118]
Adnan et al.	Nanodiamond and silver	Water	Up to 0.2% vol.	The thermal conductivity of the silver/water nanofluids was higher than that of the nanodiamond/water nanofluid. The effective density and heat capacity increased with growing concentrations of the nanofluids.	[119]
Jamshed	Hybrid copper–silver and copper	Ethylene glycol	0.09% and 0.18% vol.	The hybrid copper–silver/ethylene glycol nanofluid exhibited a higher heat transfer rate than that attained with the copper/ethylene glycol nanofluid. The thermal efficiency of the hybrid nanofluid surpassed the one of the mono nanofluid in between 2.6% and 4.4%.	[120]
Salawu et al.	Cobalt Ferrite–Copper	Ethylene Glycol	0.09% vol., 0.15% vol., and 0.18% vol.	The cobalt ferrite–copper/ethylene glycol nanofluid had higher thermal conductivity than the copper–ethylene glycol nanofluid. The energy optimization of the system was enhanced with increasing concentrations of nanoparticles. The heat transmission amount was strongly increased with increasing sizes of the nanoparticles.	[121]
Jamshed et al.	Hybrid copper–silica and copper	Ethylene glycol	---	The heat transmission was enhanced because of the amplification of thermal radiative flow and variant thermal conductivity. The hybrid nanofluid exhibited better heat transmission capability. The thermal efficiency of the copper–silica/ethylene glycol nanofluid was higher than that of the copper/ethylene glycol nanofluid in between 0.2% and 3.9%.	[122]

5. Conclusions and Future Perspectives

Advanced engineered materials enabled the exploration of space and the evolution of plane travel, but now, a new generation of materials is required to facilitate new space exploration. Nanomaterials can provide unique properties such as a large surface area, high aspect ratio, highly anisotropic and tailorable electrical and thermal conductivities, as well as optical properties, indicating that several nanomaterials can be applied to improve flexibility with maintained mechanical strength; multicomponent monitoring with redundant backup sensors; efficient power production, storage, and transmission; enhanced radiation protection for electronics and people; and sustainable life-support systems for long-duration explorations and weight reduction. Thus, the applications of advanced nanomaterials provide substantial improvements for the structures and non-structural components of almost all aeronautical and space systems, becoming a new hot field for industry.

In this review, the possible applications and interest of nanomaterials in aerospace applications were highlighted and discussed. The current state of the art on nanomaterials for heat transfer and the remaining challenges and architectures at each point where they could make difference were described. Table 2 shows the reported nanomaterials in aerospace applications. For instance, it shows that silica nanoparticles have been employed to enhance stability at high temperatures in materials intended for thermal insulation, aiming to improve material properties under elevated temperatures. The utilization of graphene and carbon nanotubes has been applied to materials where the enhancement of both thermal and electrical properties is desired. TiO_2 exhibits diverse and attractive characteristics, making it suitable for improving passive radiation and enhancing the performance of insulating materials at high temperatures.

Table 2. Matrix material, nanoparticles used, and application.

Matrix	Nanoparticle Type	Application	Ref.
Li_2SiO_3 + ZnO	SiO_2	Thermal control	[64]
Carbon/carbon	SiO_2	Improved stability at high temperatures	[85]
Acrylic resin	TiO_2	Improved passive radiative cooling performance	[90]
SiO_2	ZnO QDs	Thermal control	[6]
Alumina	Al_2O_3	Thermal control	[103]
Resole-based phenolic resin, carbon–phenolic composite, and polymer matrix composite	Carbon nanotubes, nano-diamonds, graphene oxide, $ZrSi_2$, cenosphere, and nano-SiO_2	Thermal protection	[82]
SiO_2	Ag	Lightweight, flexible pressure sensor	[87]
Cu-Cr-Y alloy	Y_2O_3 and Cr	Heat dissipation	[86]
Siliconoxycarbide–phenolic-interpenetrating aerogel	SiO_2, $ZrSi_2$, and ZrB_2	Thermal protection	[98]
Epoxy resin	Graphene nanoplatelets and carbon nanotubes	Enhanced mechanical and electrical carbon fiber composite	[123]
Epoxy resin	Graphene oxide–carbon nanotubes nanostructures decorated with nickel nanoparticles (NiGNTs)	Spacecraft structures	[91]
Poly(ether ether ketone) (PEEK)	Ag nanoparticles-decorated GO/CNT (AgGNT)	Critical aerospace applications and advanced structural composites	[91]
SiCN aerogel	TiO_2 nanorods	High-temperature, high-strength, lightweight spacecraft-insulating systems	[11]

Table 2. *Cont.*

Matrix	Nanoparticle Type	Application	Ref.
Silica aerogel with aluminum Sol-Al(H_2PO_4)$_3$	Hydroxyapatite (HAP) nanowires	Thermal protection	[10]
Jute/thermoplastic starch (TPS)	Nano-silica particles	Thermal protection	[96]
Carbon fiber/PEEK	Graphene	Thermal control	[8]
Epoxy resin	Sulfonated SiO_2	Spacecraft structures	[92]
Epoxy resin	SiO_2 and ZrO_2	Honeycomb structures	[93]
Epoxy and Kevlar 29	SiC and TiO_2	Increase flame resistance	[97]
Epoxy resin	Graphene platelet and carbon nanotube with boron nitride nanosheet	Thermal control and electric conductivity	[9]

The application of nanoparticles in heat exchangers presents an intriguing possibility in space that complicates its implementation on Earth: the absence of gravity implies a lack of sedimentation. However, this is not the sole risk associated with particle presence: phenomena such as agglomeration and adherence to walls, wicks, and other components can compromise the expected thermal gains with the addition of nanoparticles, potentially affecting the operation of these devices by obstructing a tube or impacting the heat exchange capacity in evaporation and condensation zones.

Given that active thermal control methods are already avoided in space environments due to the higher risk of failure and obvious maintenance constraints, these should not be the pioneering devices for the application of nanofluids in space missions, even though there may eventually be superior performance gains compared to passive systems. Due to their simplicity combined with high performance, systems such as pool boiling, PCM, or wickless heat pipes, e.g., pulsating heat pipes, have a much greater potential for application due to the almost negligible risk of issues such as mass adherence to one of the walls where heat exchange occurs. However, this risk may not be significant if the nanoparticles are made from excellent conductive materials, such as copper or graphene.

Another barrier to overcome is the difficulty of testing the performance of these heat exchangers, considering the challenges of simulating gravity or sending experiments into space. Even numerical simulations have serious limitations, especially in biphasic fluids. The use of devices that perform independently of gravity conditions, such as pulsating heat pipes, allows for greater reliability in gains with the use of nanofluids and can expedite the adoption of this technology by reducing testing costs.

By gathering the information available in the literature and discussed in this review, Figure 13 presents a schematic overview of the different thermal control and heat transfer mechanisms and nanoparticles applied for critical temperature control in aerospace domains and applications, including engine and propulsion systems, electronic devices, survival cells, space nuclear reactors, structures, and batteries. Both active and passive methods have been commonly implemented to achieve temperature control. Nevertheless, it can be verified that there is a common trend in the use of passive heat pipes and active radiators for multiple temperature control purposes, as well as thermal coatings and structural materials for optimal thermal protection, combined with different sets of metals, semi-metals, or carbon-based nanomaterials. This opens up a world of opportunities to optimize thermal control systems, not only focusing the well-known heat transfer mechanisms but mainly exploring novel nanomaterials and their integration into those systems.

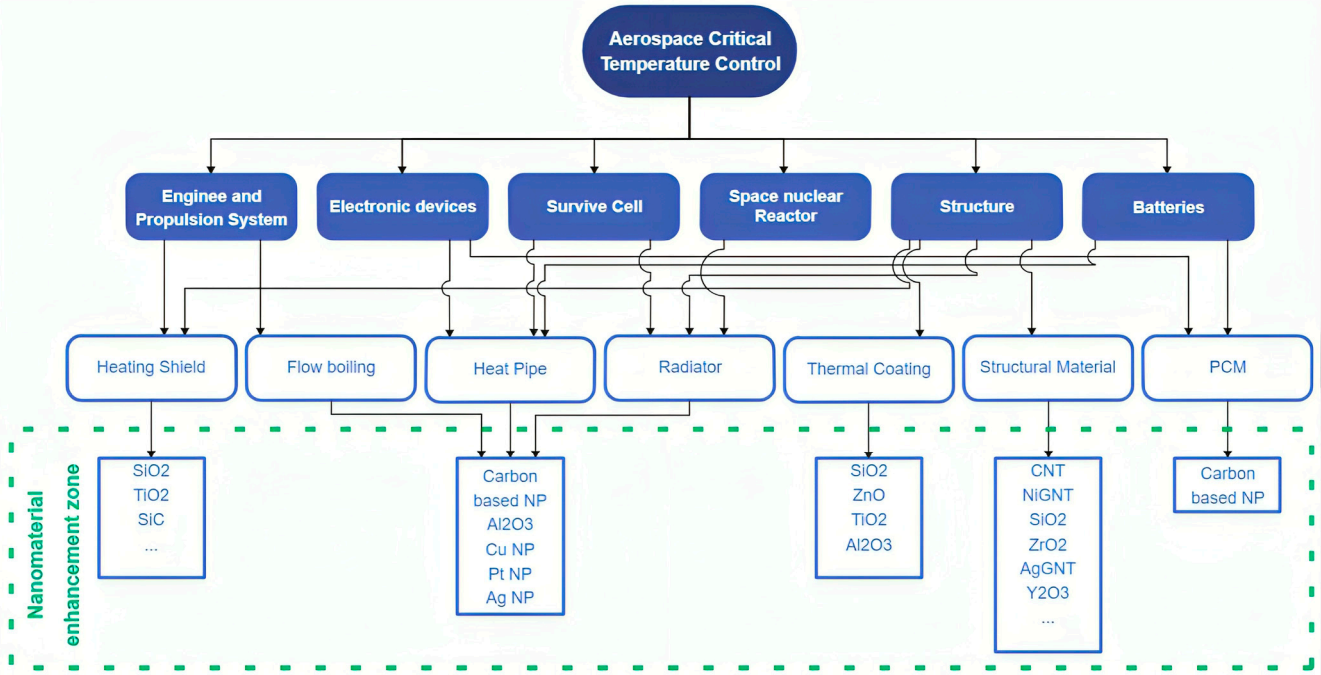

Figure 13. Overview of the main categories and nanomaterials for critical temperature control in aerospace applications.

The nanomaterials opportunities for the aerospace industry are through thermal barrier—nanofluids and wear-resistant coatings—nanoparticles; sensors that can perform safety inspections cost-effectively, quickly, and efficiently; sensors that can perform at high temperatures and other physical and chemical sensors; and composites, wear-resistant tires, improved avionics, satellites, and communication and radar technologies [123]. To improve the developments in nanomaterials aerospace applications, microfluidic technology has been mainly focused on three areas: aerodynamic flow control in vehicles, micropower generators (fuel cells and microturbines), and micropropulsion devices [124,125]. Considerable work has also been developed on microfluidic devices for extraterrestrial applications such as advanced environmental control and life-support systems–lab-on-chip systems [102,103]. Examples include microfluidic systems for temperature and humidity control in spacecrafts, trace contaminant monitoring and removal, water quality monitoring, and in vitro physiological monitoring and drug delivery devices [124–127]. Microfluidic systems have a significant advantage over conventional systems in terms of space, power, and weight requirements, which are a premium in aerospace applications. Although the need for advances in automation, smaller set-ups (micropumps, valves), robust integrations, and materials (microphysiological systems, membranes, filters) for small footprints (3D printing, bioprinting) are still needed.

Thus, microfluidics technology can have a large impact on future developments in the aerospace industry and its applications. In the area of aerodynamics, microfluidics will have applications in the design of aerodynamic surfaces such as wings, control surfaces, jet noise control, and flow in turbomachinery [127]. Micropropulsion devices will be used for satellite attitude corrections and formation flights of micro- to femto-sized satellites [127]. High-energy-density micropower generation devices, such as fuel cells, will consist of microfluidic components and thermal management devices.

Several studies of microphysiological systems in the aerospace environment have also demonstrated that these two areas combined can bring new insights to personalized medicine and faster understanding and developments in new nanomaterials for medicine applications, such as for drug deliveries or disease modelling for new approaches [128] in space medicine.

Thus, numerous nanomaterials developments have improved their applications in aerospace; therefore, microfluidic-based studies can provide better and innovative ways to understand where they can improve their properties and to conduct compressive understandings of their behavior in such different environments. The exploitation of these opportunities and finding solutions to the associated challenges between nanofluids and microfluidic technologies, for aerospace, will rely on highly effective partnerships for commercial development, scientific innovation, systems engineering, design, and manufacturing.

As recommendations for further studies, the authors suggest incorporating different parameters into the flow performance, at greater levels of the thermal conductivity parameter, considering factors like second-order slip, activation energy, and magneto slip. More works should be conducted on the heat transfer performance of liquid droplet radiators, with the possible technological development of this type of radiator being one of the most promising solutions in terms of performance and efficient coupling with aerospace energy conversion systems. The development of the liquid sheet radiators should be based on the configuration of the sheets in parallel, working at distinct mean temperatures, and a reduction in the volume of the single components to decrease the amount of fluid used in the radiator. Solutions based on microchannel heat exchangers should be further explored. They are beneficial for the aerospace thermal management systems due to their improved heat transfer, low weight, and material and energy savings compared to the traditional heat exchangers. Also, further studies should be performed at the bubble scale to analyze the local heat and mass transfer around the bubble and at its base and the bubble departure underlying mechanisms under the action of electric/magnetic fields or shear flows in parabolic flights. These studies should incorporate complementary approaches based on normal and microgravity experiments, the development of theoretical models, and direct numerical simulations. Additionally, it is recommended to focus research efforts on obtaining accurate databases on flow boiling and condensation under microgravity scenarios. In this scope, more experimentally validated models for the flow boiling CHF in microgravity and criteria to predict the minimum flow rate required to ensure gravity-independent CHF should be further developed. In terms of condensation, it is recommended to develop an experimentally validated model for condensation in microgravity and criteria to estimate the minimum flow rate necessary to ensure gravity-independent annular condensation. Despite the extensive data available in the literature, it is shown that there is a considerable scarcity of useful correlations and models that may compromise the readiness to adopt flow boiling in space thermal management systems. Furthermore, the two main factors that determine the energy balance of spacecraft are the change in the external thermal radiation environment and the operation mode of the internal equipment. Most of the research on thermal management regards the operation of each piece of equipment as independent, and the external environment of spacecraft generally takes several typical environments, but the operation of spacecraft is a dynamic process. In the systematic design of spacecraft thermal management, the dynamic processes of the whole system should be considered, and the restrictions and joint relations of each dynamic process should be fully studied. It is recommended to further study the technological solutions based on innovative phase change materials and highly thermal conductive materials for passive thermal control to fully recover and use the heat of electronic equipment to attain the local heat balance, significantly reducing the energy requirements for thermal regulation. More research should also be conducted on novel thermal control coatings and multilayer insulation materials. The thermal radiation parameters of thermal control coating directly determine the energy exchange between the spacecraft and the space environment. The exploration of smart thermal control coatings may regulate the energy transfer and removal of spacecraft from whole to part and greatly improve the performance of the spacecraft. Also, we welcome further research and the application of innovative multilayered insulation materials with enhanced performance in vacuum insulation, enabling them to attain high strength and energy storage capability.

Author Contributions: Conceptualization, G.N., B.C., R.S., J.P. and D.P.; writing—original draft preparation, G.N., B.C., R.S., J.P. and D.P.; writing—review and editing, G.N., B.C., R.S., J.P., P.P., S.O.C., D.P., A.M. and R.L.; supervision, A.M. and R.L. All authors have read and agreed to the published version of the manuscript.

Funding: This work has been funded by FCT/MCTES (PIDDAC) through the base funding from the following research units: UIDP/50009/2020-FCT and UIDB/50009/2020-FCT, UIDB/00532/2020, LA/P/0045/2020, UIDB/04077/2020, and UIDP/04077/2020. The authors are also grateful for FCT funding through 2022. 03151.PTDC, PTDC/EME-TED/7801/2020, POCI-01-0145-FEDER-016861, POCI-01-0145-FEDER-028159, 2022. 02085.PTDC (https://doi.org/10.54499/2022.02085.PTDC, accessed on 25 March 2024), funded by COMPETE2020, NORTE2020, PORTUGAL2020, and FEDER. Glauco Nobrega was supported by the doctoral grant PRT/BD/153088/2021, financed by the Portuguese Foundation for Science and Technology (FCT), under the MIT Portugal Program. Pinho D. and Susana O. Catarino thank FCT for her contract funding provided through 2021.00027.CEECIND, 2020.00215.CEECIND (DOI: https://doi.org/10.54499/2020.00215.CEECIND/CP1600/CT0009, accessed on 25 March 2024), respectively. The authors are also grateful to the Fundação para a Ciência e a Tecnologia (FCT), Avenida D. Carlos I, 126, 1249–074 Lisboa, Portugal, for partially financing the Project "Estratégias interfaciais de arrefecimento para tecnologias de conversão com elevadas potências de dissipação", ref. PTDC/EMETED/7801/2020, Associação do Instituto Superior Técnico para a Investigação e o Desenvolvimento (IST-ID). José Pereira also acknowledges FCT for his PhD fellowship (Ref. 2021. 05830.BD). The authors are also grateful for FCT funding through 2022.03151.PTD and LA/P/0083/2020 IN + -IST-ID. The authors are also grateful for FCT funding through 2022.03151.PTD and LA/P/0083/2020 IN + -IST-ID and through UIPD/50009/2020-FCT and UIDB/50009—FCT. Ana Moita also acknowledges FCT for partially financing her contract through CEECINST/00043/2021/CP2797/CT0005, doi:https://doi.org/10.54499/CEECINST/00043/2021/CP2797/CT0005, accessed on 25 March 2024. The authors also acknowledge Exército Português for their support through projects CINAMIL Desenvolvimento de Sistemas de Gestão Térmica e Climatização de equipamento NBQ and COOLUAV—Sistema de arrefecimento da componente eletrónica e baterias em veículos militares não tripulados.

Data Availability Statement: No new data were created or analyzed in this study. Data sharing is not applicable to this article.

Conflicts of Interest: The authors declare no conflicts of interest.

References

1. Gilmore, D.G. *Spacecraft Thermal Control Handbook, Volume I: Fundamental Technologies*; AIAA: Reston, WV, USA, 2002.
2. Hibbs, A.R. NASA Space Science Data Coordinated Archive. Available online: http://nssdc.gsfc.nasa.gov (accessed on 25 March 2024).
3. Ali, H.M. Applications of combined/hybrid use of heat pipe and phase change materials in energy storage and cooling systems: A recent review. *J. Energy Storage* **2019**, *26*, 100986. [CrossRef]
4. Alami, A.H.; Ramadan, M.; Tawalbeh, M.; Haridy, S.; Al Abdulla, S.; Aljaghoub, H.; Ayoub, M.; Alashkar, A.; Abdelkareem, M.A.; Olabi, A.G. A critical insight on nanofluids for heat transfer enhancement. *Sci. Rep.* **2023**, *13*, 15303. [CrossRef] [PubMed]
5. Yang, Q.; Zhao, L.; Yu, H.; Min, Q.; Chen, C.; Zhou, D.; Yu, X.; Qiu, J.; Li, B.; Xu, X. UV-shielding device of high-stability glass embedded with in-situ growth of ZnO quantum dots. *J. Alloys Compd.* **2019**, *784*, 535–540. [CrossRef]
6. Chen, J.; Yu, Y.; Feng, A.; Mi, L.; Xiu, H.; Yu, Y. Optical properties and radiation stability of SiO_2/ZnO composite pigment prepared by co-sintering method. *Ceram. Int.* **2022**, *48*, 754–759. [CrossRef]
7. Hu, C.; Zhang, H.; Neate, N.; Fay, M.; Hou, X.; Grant, D.; Xu, F. Highly Aligned Ni-Decorated GO–CNT Nanostructures in Epoxy with Enhanced Thermal and Electrical Properties. *Polymers* **2022**, *14*, 2583. [CrossRef] [PubMed]
8. Leow, C.; Kreider, P.B.; Sommacal, S.; Kluth, P.; Compston, P. Electrical and thermal conductivity in graphene-enhanced carbon-fibre/PEEK: The effect of interlayer loading. *Carbon* **2023**, *215*, 118463. [CrossRef]
9. Wang, S.; Cao, M.; Cong, F.; Xue, H.; Li, X.; Zhao, C.; Cui, X. Mechanical and thermal properties of graphene and carbon nanotube reinforced epoxy/boron nitride adhesives. *J. Adhes. Sci. Technol.* **2021**, *35*, 2142–2158. [CrossRef]
10. Kong, D.; Li, H.; Gao, Y.; He, L.; Ji, X.; Zhang, F.; Li, W.; Zhang, H. Preparation and Characteristic of the Novel Multiple-Layer Thermal Insulation Nanocomposite Materials. *ACS Sustain. Chem. Eng.* **2023**, *11*, 11067–11076. [CrossRef]
11. Wang, J.; Li, H.; Liu, H.; Feng, Z.; Cui, Z.; Liao, X.; Zhang, B.; Li, Q. Polar bear hair inspired ternary composite ceramic aerogel with excellent interfacial bonding and efficient infrared transmittance for thermal insulation. *J. Eur. Ceram. Soc.* **2023**, *43*, 4927–4938. [CrossRef]
12. Kuprat, J.; van der Broeck, C.H.; Andresen, M.; Kalker, S.; Liserre, M.; De Doncker, R.W. Research on Active Thermal Control: Actual Status and Future Trends. *IEEE J. Emerg. Sel. Top. Power Electron.* **2021**, *9*, 6494–6506. [CrossRef]

13. Calvert, M.J.; Baker, J. Micro-scale transport—Non-continuum thermophysical property variation effects on heat and momentum transfer. *J. Thermophys. Heat Transf.* **1998**, *12*, 138. [CrossRef]
14. Tien, C.L.; Cunnington, G.R. *Advances in Heat Transfer*; Hartnett, J.P., Irvine, T.F., Eds.; Academic: New York, NY, USA, 1973.
15. Zhao, L.; Rezkallah, K.S. Gas-liquid flow patterns at microgravity conditions. *Int. J. Multiph. Flow* **1993**, *19*, 751–763. [CrossRef]
16. Xiong, Y.; Guo, L.; Huang, Y.; Chen, L.H. Intelligent Thermal Control Strategy Based on Reinforcement Learning for Space Telescope. *J. Thermophys. Heat Transf.* **2020**, *34*, 37–44. [CrossRef]
17. NASA. *Active Thermal Control System (ATCS) Overview*; National Aeronautics and Space Administration (NASA): Washington, DC, USA, 2021. Available online: https://www.nasa.gov/wp-content/uploads/2021/02/473486main_iss_atcs_overview.pdf (accessed on 25 March 2024).
18. Ungar, E.; Erickson, L. Assessment of the Use of Nanofluids in Spacecraft Active Thermal Control Systems. In *AIAA SPACE 2011 Conference & Exposition*; AIAA SPACE Forum; American Institute of Aeronautics and Astronautics: Reston, WV, USA, 2011.
19. Wang, T.; Zhang, L.; Zhang, F.; Lu, Y. Reduction and reconstruction strategy of active thermal control system based on unsupervised learning and thermo-optics for spaceborne high-resolution remote sensor. *Appl. Therm. Eng.* **2023**, *230*, 120676. [CrossRef]
20. Li, S.; Wang, Y.; Zhang, H.; Yu, F. Thermal Analysis and Validation of GF-4 Remote Sensing Camera. *J. Therm. Sci.* **2020**, *29*, 992–1000. [CrossRef]
21. Meng, Q.; Wang, D.; Wang, X.; Li, W.; Yang, X.; Yan, D.; Li, Y.; Cao, Z.; Ji, Q.; Sun, T.; et al. High Resolution Imaging Camera (HiRIC) on China's First Mars Exploration Tianwen-1 Mission. *Space Sci. Rev.* **2021**, *217*, 42. [CrossRef]
22. Ortega, D.; Amador, A.; Ahmad, M.; Choudhuri, A.; Rahman, M.M. Liquid Nitrogen Flow Boiling Critical Heat Flux in Additively Manufactured Cooling Channels. *Aerospace* **2023**, *10*, 499. [CrossRef]
23. Inoue, K.; Ohta, H.; Toyoshima, Y.; Asano, H.; Kawanami, O.; Imai, R.; Suzuki, K.; Shinmoto, Y.; Matsumoto, S. Heat Loss Analysis of Flow Boiling Experiments Onboard International Space Station with Unclear Thermal Environmental Conditions (1st Report: Subcooled Liquid Flow Conditions at Test Section Inlet). *Microgravity Sci. Technol.* **2021**, *33*, 28. [CrossRef]
24. Devahdhanush, V.S.; Darges, S.J.; Mudawar, I.; Nahra, H.K.; Balasubramaniam, R.; Hasan, M.M.; Mackey, J.R. Flow visualization, heat transfer, and critical heat flux of flow boiling in Earth gravity with saturated liquid-vapor mixture inlet conditions—In preparation for experiments onboard the International Space Station. *Int. J. Heat Mass Transf.* **2022**, *192*, 122890. [CrossRef]
25. Mudawar, I.; Lee, J. Experimental and computational investigation into hydrodynamic and heat transfer characteristics of subcooled flow boiling on the International Space Station. *Int. J. Heat Mass Transf.* **2023**, *207*, 124000. [CrossRef]
26. Han, Z.; Zhang, J.; Wang, M.; Tian, W.; Qiu, S.; Su, G.H. A modified system analysis code for thermo-hydraulic calculation of hydrogen in a nuclear thermal propulsion (NTP) system. *Ann. Nucl. Energy* **2021**, *164*, 108632. [CrossRef]
27. Zhang, Y.-N.; Zhang, H.-C.; Zhang, X.; Yu, H.-X.; Zhao, G.-B. Block Radial Basis Function Collocation Meshless method applied to steady and transient neutronics problem solutions in multi-material reactor cores. *Prog. Nucl. Energy* **2018**, *109*, 83–96. [CrossRef]
28. El-Genk, M.S. Space nuclear reactor power system concepts with static and dynamic energy conversion. *Energy Convers. Manag.* **2008**, *49*, 402–411. [CrossRef]
29. Lee, K.-L.; Tarau, C.; Anderson, W.G.; Beard, D. Titanium-Water Heat Pipe Radiators for Space Fission Power System Thermal Management. *Microgravity Sci. Technol.* **2020**, *32*, 453–464. [CrossRef]
30. Li, Z.; Zhang, H.; Huang, Z.; Zhang, D.; Wang, H. Characteristics and optimation of heat pipe radiator for space nuclear propulsion spacecraft. *Prog. Nucl. Energy* **2022**, *150*, 104307. [CrossRef]
31. Zhao, C.; Huang, Y.; Wang, J. Solid particle radiator systems for heat rejection in space. *J. Phys. Conf. Ser.* **2021**, *1777*, 012054. [CrossRef]
32. Kianfar, K.; Joodaki, S.; Dashti, I.; Asghari, S. Lifetime estimation of heat pipes in space applications using particle filtering, Arrhenius and FIDES methods. *Therm. Sci. Eng. Prog.* **2021**, *22*, 100847. [CrossRef]
33. Mohamed, H.A.E.; Ezzaldeen, E. Heat Pipes for Computer Cooling Applications. In *Electronics Cooling*; Murshed, S.M.S., Ed.; IntechOpen: Rijeka, Republic of Croatia, 2016; Chapter 4.
34. Senthil, R.; Madurai Elavarasan, R.; Pugazhendhi, R.; Premkumar, M.; Vengadesan, E.; Navakrishnan, S.; Islam, M.R.; Natarajan, S.K. A holistic review on the integration of heat pipes in solar thermal and photovoltaic systems. *Sol. Energy* **2021**, *227*, 577–605. [CrossRef]
35. Shukla, K. Heat Pipe for Aerospace Applications—An Overview. *J. Electron. Cool. Therm. Control.* **2015**, *5*, 1–14. [CrossRef]
36. Mock, P.R.; Marcus, D.B.; Edelman, E.A. Communications Technology Satellite: A Variable Conductance Heat Pipe Application. *J. Spacecr. Rocket.* **1975**, *12*, 750–753. [CrossRef]
37. Kim, T.Y.; Hyun, B.-S.; Lee, J.-J.; Rhee, J. Numerical study of the spacecraft thermal control hardware combining solid–liquid phase change material and a heat pipe. *Aerosp. Sci. Technol.* **2013**, *27*, 10–16. [CrossRef]
38. Zhao, X.; Su, L.; Jiang, J.; Deng, W.; Zhao, D. A Review of Working Fluids and Flow State Effects on Thermal Performance of Micro-Channel Oscillating Heat Pipe for Aerospace Heat Dissipation. *Aerospace* **2023**, *10*, 179. [CrossRef]
39. Ababneh, M.T.; Tarau, C.; Anderson, W.G.; Farmer, J.T.; Hawkins, R.; Alvarez-Hernandez, A.R.; Ortega, S.; Fisher, J.W. Copper-Water and Hybrid Aluminum-Ammonia Heat Pipes for Spacecraft Thermal Control Applications. In Proceedings of the International Heat Pipe Symposium (IHPS), Pisa, Italy, 10–14 June 2018.
40. Hu, L.; Chen, Z.; Shi, K.; Shi, J.; Luo, X.; Liu, C. Sodium/GH4099 Heat Pipes for Space Reactor Cooling. *Microgravity Sci. Technol.* **2021**, *33*, 60. [CrossRef]

41. Mameli, M.; Araneo, L.; Filippeschi, S.; Marelli, L.; Testa, R.; Marengo, M. Thermal response of a closed loop pulsating heat pipe under a varying gravity force. *Int. J. Therm. Sci.* **2014**, *80*, 11–22. [CrossRef]
42. Ando, M.; Okamoto, A.; Tanaka, K.; Maeda, M.; Sugita, H.; Daimaru, T.; Nagai, H. On-orbit demonstration of oscillating heat pipe with check valves for space application. *Appl. Therm. Eng.* **2018**, *130*, 552–560. [CrossRef]
43. Ayel, V.; Araneo, L.; Marzorati, P.; Romestant, C.; Bertin, Y.; Marengo, M. Visualization of Flow Patterns in Closed Loop Flat Plate Pulsating Heat Pipe Acting as Hybrid Thermosyphons under Various Gravity Levels. *Heat Transf. Eng.* **2019**, *40*, 227–237. [CrossRef]
44. Pereira, J.; Souza, R.; Moreira, A.; Moita, A. A Review on the Nanofluids-PCMs Integrated Solutions for Solar Thermal Heat Transfer Enhancement Purposes. *Technologies* **2023**, *11*, 166. [CrossRef]
45. Torres-Rodríguez, A.; Morillón-Gálvez, D.; Aldama-Ávalos, D.; Hernández-Gómez, V.H.; García Kerdan, I. Thermal performance evaluation of a passive building wall with CO_2-filled transparent thermal insulation and paraffin-based PCM. *Sol. Energy* **2020**, *205*, 1–11. [CrossRef]
46. Khadem, Z.; Salari, A.; Naghdbishi, A.; Shakibi, H.; Sardarabadi, M. Parametric analysis of a PCM-based heat sink for electronic device thermal management. *J. Energy Storage* **2023**, *74*, 109118. [CrossRef]
47. Collette, J.; Rochus, P.; Peyrou-Lauga, R.; Pin, O.; Nutal, N.; Larnicol, M.; Crahay, J. Phase change material device for spacecraft thermal control. In *Proceedings of the 62nd International Astronautical Congress 2011, IAC 2011, Cape Town, South Africa, 3–7 October 2011*; International Astronautical Federation: Paris, France, 2011; Volume 7, pp. 6020–6031.
48. Huibin, Y.; Xuenong, G.; Jing, D. Cooling technology of electronic device based on phase-change material with rapid thermal response. *J. South Chin. Univ. Technol. (Nat. Sci. Ed.)* **2007**, *35*, 52–56.
49. Lafdi, K.; Mesalhy, O.; Elgafy, A. Graphite foams infiltrated with phase change materials as alternative materials for space and terrestrial thermal energy storage applications. *Carbon* **2008**, *46*, 159–168. [CrossRef]
50. He, Y.; Tao, Y.B.; Zhao, C.Y.; Yu, X.K. Structure parameter analysis and optimization of photovoltaic-phase change material-thermoelectric coupling system under space conditions. *Renew. Energy* **2022**, *200*, 320–333. [CrossRef]
51. Borshchak Kachalov, A.; Salgado Sánchez, P.; Martínez, U.; Ezquerro, J.M. Preliminary Design of a Space Habitat Thermally Controlled Using Phase Change Materials. *Thermo* **2023**, *3*, 232–247. [CrossRef]
52. Garmendia, I.; Vallejo, H.; Seco, M.; Anglada, E. Design and Fabrication of a Phase Change Material Heat Storage Device for the Thermal Control of Electronics Components of Space Applications. *Aerospace* **2022**, *9*, 126. [CrossRef]
53. Zmywaczyk, J.; Zbińkowski, P.; Koniorczyk, P. Thermophysical Properties of POLWAX LTP ST Paraffin Doped with or without Carbon Nanotubes or Silver Nanowires and Passive Cooling of a High-Power LED Panel. *Energies* **2023**, *16*, 6068. [CrossRef]
54. Khan, Z.; Khan, Z.A. Experimental and numerical investigations of nano-additives enhanced paraffin in a shell-and-tube heat exchanger: A comparative study. *Appl. Therm. Eng.* **2018**, *143*, 777–790. [CrossRef]
55. Krishna, J.; Kishore, P.S.; Solomon, A.B. Heat pipe with nano enhanced-PCM for electronic cooling application. *Exp. Therm. Fluid Sci.* **2017**, *81*, 84–92. [CrossRef]
56. Attinger, D.; Frankiewicz, C.; Betz, A.R.; Schutzius, T.M.; Ganguly, R.; Das, A.; Kim, C.-J.; Megaridis, C.M. Surface engineering for phase change heat transfer: A review. *MRS Energy Sustain.* **2014**, *1*, 4. [CrossRef]
57. Nukiyama, S. The maximum and minimum values of the heat Q transmitted from metal to boiling water under atmospheric pressure. *Int. J. Heat Mass Transf.* **1966**, *9*, 1419–1433. [CrossRef]
58. Kondo, M.; Matsumoto, J. Surface tension and wettability calculation using density gradient potential in a physically consistent particle method. *Comput. Methods Appl. Mech. Eng.* **2021**, *385*, 114072. [CrossRef]
59. Garivalis, A.I.; Manfredini, G.; Saccone, G.; Di Marco, P.; Kossolapov, A.; Bucci, M. Critical heat flux enhancement in microgravity conditions coupling microstructured surfaces and electrostatic field. *npj Microgravity* **2021**, *7*, 37. [CrossRef] [PubMed]
60. Dhir, V.K.; Warrier, G.R.; Aktinol, E.; Chao, D.; Eggers, J.; Sheredy, W.; Booth, W. Nucleate Pool Boiling Experiments (NPBX) on the International Space Station. *Microgravity Sci. Technol.* **2012**, *24*, 307–325. [CrossRef]
61. Quintana-Buil, G.; González-Cinca, R. Acoustic effects on heat transfer on the ground and in microgravity conditions. *Int. J. Heat Mass Transf.* **2021**, *178*, 121627. [CrossRef]
62. Moehrle, R.E.; Chung, J.N. Pool boiling heat transfer driven by an acoustic standing wave in terrestrial gravity and microgravity. *Int. J. Heat Mass Transf.* **2016**, *93*, 322–336. [CrossRef]
63. Zhang, Y.; Zhao, J.; Wei, J.; Xue, Y. Nucleate Pool Boiling Heat Transfer on a Micro-Pin-Finned Surface in Short-Term Microgravity. *Heat Transf. Eng.* **2017**, *38*, 594–610. [CrossRef]
64. Zhang, Y.; Wei, J.; Xue, Y.; Kong, X.; Zhao, J. Bubble dynamics in nucleate pool boiling on micro-pin-finned surfaces in microgravity. *Appl. Therm. Eng.* **2014**, *70*, 172–182. [CrossRef]
65. Gajanan, K.; Tijare, S.N. Applications of nanomaterials. *Mater. Today Proc.* **2018**, *5 Pt 1*, 1093–1096. [CrossRef]
66. Pathak, S.; Saha, G.C.; Abdul Hadi, M.B.; Jain, N.K. Engineered Nanomaterials for Aviation Industry in COVID-19 Context: A Time-Sensitive Review. *Coatings* **2021**, *11*, 382. [CrossRef]
67. Hu, C.; Liu, T.; Neate, N.; Fay, M.; Hou, X.; Grant, D.; Xu, F. Enhanced thermal and electrical properties by Ag nanoparticles decorated GO–CNT nanostructures in PEEK composites. *Compos. Sci. Technol.* **2022**, *218*, 109201. [CrossRef]
68. Farzanehfar, N.; Taheri, A.; Rafiemanzelat, F.; Jazani, O.M. High-performance epoxy nanocomposite adhesives with enhanced mechanical, thermal and adhesion properties based on new nanoscale ionic materials. *Chem. Eng. J.* **2023**, *471*, 144428. [CrossRef]

69. Kaveh, A.; Moini Jazani, O.; Fallahi, M.; Asghari, S.; Mirmohammadi, S.M.; Hajizamani, E.; Taghavi, M.R.; Namvar Asl, A. Introducing a new approach for designing advanced epoxy film adhesives with high mechanical, adhesion, and thermal properties by adding hybrid additives for structural bonding. *Colloids Surf. A Physicochem. Eng. Asp.* **2023**, *676*, 132180. [CrossRef]
70. Shekar, R.I.; Kotresh, T.M.; Rao, P.M.D.; Kumar, K. Properties of high modulus PEEK yarns for aerospace applications. *J. Appl. Polym. Sci.* **2009**, *112*, 2497–2510. [CrossRef]
71. Akibul Islam, M.; Chowdhury, M.A.; Arefin Kowser, M.; Osman Ali, M.; Azad, K.; Ramjan Ali, M. Enhancement of thermal properties of Kevlar 29 coated by SiC and TiO_2 nanoparticles and their binding energy analysis. *Arab. J. Chem.* **2022**, *15*, 103959. [CrossRef]
72. Azad, M.M.; Ejaz, M.; Shah, A.U.R.; Afaq, S.K.; Song, J.-I. A bio-based approach to simultaneously improve flame retardancy, thermal stability and mechanical properties of nano-silica filled jute/thermoplastic starch composite. *Mater. Chem. Phys.* **2022**, *289*, 126485. [CrossRef]
73. Delfini, A.; Pastore, R.; Santoni, F.; Piergentili, F.; Albano, M.; Alifanov, O.; Budnik, S.; Morzhukhina, A.; Nenarokomov, A.; Titov, D. Thermal analysis of advanced plate structures based on ceramic coating on carbon/carbon substrates for aerospace Re-Entry Re-Useable systems. *Acta Astronaut.* **2021**, *183*, 153–161. [CrossRef]
74. Wang, Y.; Ba, F.; Chai, Z.; Zhang, Z. A review of thermal control coatings prepared by micro-arc oxidation on light alloys. *Int. J. Electrochem. Sci.* **2024**, *19*, 100514. [CrossRef]
75. Peltier, F.; Thierry, D. Review of Cr-Free Coatings for the Corrosion Protection of Aluminum Aerospace Alloys. *Coatings* **2022**, *12*, 518. [CrossRef]
76. Zareanshahraki, F.; Asemani, H.R.; Skuza, J.; Mannari, V. Synthesis of non-isocyanate polyurethanes and their application in radiation-curable aerospace coatings. *Prog. Org. Coat.* **2020**, *138*, 105394. [CrossRef]
77. Chen, G.; Wang, Y.; Qiu, J.; Cao, J.; Zou, Y.; Wang, S.; Jia, D.; Zhou, Y. Robust Inorganic Daytime Radiative Cooling Coating Based on a Phosphate Geopolymer. *ACS Appl. Mater. Interfaces* **2020**, *12*, 54963–54971. [CrossRef]
78. Sharma, A.K. Surface engineering for thermal control of spacecraft. *Surf. Eng.* **2005**, *21*, 249–253. [CrossRef]
79. Mikhailov, M.; Yuryev, S.; Lapin, A.; Goronchko, V. Reflective thermal control coating for spacecraft based on ZnO pigment and Li_2SiO_3 silicate modified by SiO_2 nanoparticles. *Ceram. Int.* **2023**, *49*, 20817–20821. [CrossRef]
80. Chen, H.; Li, P.; Zhou, H.; Zhang, W.; Cong, L.; Ma, J. Full solar-spectral reflectance of ZnO QDs/SiO_2 composite pigment for thermal control coating. *Mater. Res. Bull.* **2022**, *146*, 111572. [CrossRef]
81. Chen, M.; Pang, D.; Chen, X.; Yan, H.; Yang, Y. Passive daytime radiative cooling: Fundamentals, material designs, and applications. *EcoMat* **2022**, *4*, e12153. [CrossRef]
82. Liu, J.; Zhou, Z.; Zhang, D.; Jiao, S.; Zhang, J.; Gao, F.; Ling, J.; Feng, W.; Zuo, J. Research on the performance of radiative cooling and solar heating coupling module to direct control indoor temperature. *Energy Convers. Manag.* **2020**, *205*, 112395. [CrossRef]
83. Alimohammadian, M.; Dinarvand, S. Enhancement of passive daytime radiative cooling performance with a novel hybrid strategy of integrating double-layer nanoparticle-based coating and ballistic thermal rectifier. *J. Therm. Anal. Calorim.* **2023**, *148*, 7995–8007. [CrossRef]
84. Kang, H.-K. Microstructure and electrical conductivity of high volume Al_2O_3-reinforced copper matrix composites produced by plasma spray. *Surf. Coat. Technol.* **2005**, *190*, 448–452. [CrossRef]
85. Bolelli, G.; Cannillo, V.; Lugli, C.; Lusvarghi, L.; Manfredini, T. Plasma-sprayed graded ceramic coatings on refractory materials for improved chemical resistance. *J. Eur. Ceram. Soc.* **2006**, *26*, 2561–2579. [CrossRef]
86. Sachidananda, K.B.; Mahesha, K.; Dey, A. Effect of powder particle size on vibration damping behaviour of plasma sprayed alumina (Al_2O_3) coating on AISI 304 stainless steel substrate. *Ceram. Int.* **2018**, *44*, 158–163. [CrossRef]
87. Gangil, N.; Siddiquee, A.N.; Maheshwari, S. Aluminium based in-situ composite fabrication through friction stir processing: A review. *J. Alloys Compd.* **2017**, *715*, 91–104. [CrossRef]
88. He, G.; Guo, W.; He, D.; Zhang, J.; Xing, Z.; Lv, Z.; Jia, L.; Huang, Y. Study of the Mechanical Properties and Thermal Control Performance of Plasma-Sprayed Alumina Coating on Aluminum Alloy Surface. *Appl. Sci.* **2023**, *13*, 956. [CrossRef]
89. Gogu, C.; Bapanapalli, S.K.; Haftka, R.T.; Sankar, B.V. Comparison of Materials for an Integrated Thermal Protection System for Spacecraft Reentry. *J. Spacecr. Rocket.* **2009**, *46*, 501–513. [CrossRef]
90. Allen, H.J. Hypersonic Flight and the Re-Entry Problem: The Twenty-First Wright Brothers Lecture. *J. Aerosp. Sci.* **1958**, *25*, 217–227. [CrossRef]
91. Sutton, G.P.; Biblarz, O. *Rocket Propulsion Elements*.; John Wiley & Sons: Hoboken, NJ, USA, 2016.
92. Favaloro, M. Ablative Materials. *Kirk-Othmer Encyclopedia of Chemical Technology*, Wiley Online Library: Hoboken, NJ, USA, 2000. [CrossRef]
93. Park, S.-J.; Seo, M.-K. Chapter 7—Types of Composites. In *Interface Science and Technology*; Park, S.-J., Seo, M.-K., Eds.; Elsevier: Amsterdam, The Netherlands, 2011; Volume 18, pp. 501–629.
94. Kausar, A. *Polymeric Nanocomposites with Carbonaceous Nanofillers for Aerospace Applications*; Woodhead Publishing Series in Composites Science and Engineering: Cambridge, UK, 2022.
95. Yuan, S.; Shen, F.; Chua, C.K.; Zhou, K. Polymeric composites for powder-based additive manufacturing: Materials and applications. *Prog. Polym. Sci.* **2019**, *91*, 141–168. [CrossRef]

96. Öztürkmen, M.B.; Özkutlu Demirel, M.; Ağaç, Ö.; Ece, R.E.; Öz, Y. Tailored multifunctional nanocomposites obtained by integration of carbonaceous fillers in an aerospace grade epoxy resin curing at high temperatures. *Diam. Relat. Mater.* **2023**, *135*, 109840. [CrossRef]
97. Tate, J.S.; Gaikwad, S.; Theodoropoulou, N.; Trevino, E.; Koo, J.H. Carbon/Phenolic Nanocomposites as Advanced Thermal Protection Material in Aerospace Applications. *J. Compos.* **2013**, *2013*, 403656. [CrossRef]
98. Ahmad, S.; Ali, S.; Salman, M.; Baluch, A.H. A comparative study on the effect of carbon-based and ceramic additives on the properties of fiber reinforced polymer matrix composites for high temperature applications. *Ceram. Int.* **2021**, *47*, 33956–33971. [CrossRef]
99. Tran, H.K.; Rasky, D.J.; Esfahani, L. Thermal response and ablation characteristics of lightweight ceramic ablators. *J. Spacecr. Rocket.* **1994**, *31*, 993–998. [CrossRef]
100. Kubota, Y.; Miyamoto, O.; Aoki, T.; Ishida, Y.; Ogasawara, T.; Umezu, S. New thermal protection system using high-temperature carbon fibre-reinforced plastic sandwich panel. *Acta Astronaut.* **2019**, *160*, 519–526. [CrossRef]
101. Jin, X.; Liu, C.; Huang, H.; Pan, R.; Wu, C.; Yan, X.; Wang, H.; Pan, Y.; Hong, C.; Zhang, X. Multiscale, elastic, and low-density carbon fibre/siliconoxycarbide-phenolic interpenetrating aerogel nanocomposite for ablative thermal protection. *Compos. Part B Eng.* **2022**, *245*, 110212. [CrossRef]
102. Zhou, Y.; Yin, S.; Zhou, Q.; Chen, Z.; Xue, L.; Li, H.; Yan, Y. Improving high temperature properties of Cu-Cr-Y alloy by residual Cr particles and nano-Y_2O_3 dispersions. *J. Mater. Res. Technol.* **2022**, *21*, 2976–2988. [CrossRef]
103. Wang, Z.; Cheng, Z.; Jiao, X.; Chen, D.; Wang, T. Formation of SiO_2-Encapsulated Ag Nanoparticles on SiO_2 Nanofibers and Their Application as Robust, Flexible Pressure Sensor Working under High Temperatures. *ACS Appl. Nano Mater.* **2023**, *6*, 6112–6120. [CrossRef]
104. Rahman, M.H.; Chowdhury, E.H.; Hong, S. High temperature oxidation of monolayer MoS_2 and its effect on mechanical properties: A ReaxFF molecular dynamics study. *Surf. Interfaces* **2021**, *26*, 101371. [CrossRef]
105. Martin, K.L.; Clarkson, C.M.; Thompson, C.; Germanton, G.; Posey, N.; Wiegart, L.; Ramakrishnan, S.; Dickerson, M.B. Influence of Thermal Treatment on Preceramic Polymer Grafted Nanoparticle Network Formation: Implications for Thermal Protection Systems and Aerospace Propulsion Components. *ACS Appl. Nano Mater.* **2022**, *5*, 15288–15297. [CrossRef]
106. Das, S.K.; Choi, S.U.; Yu, W.; Pradeep, T. *Nanofluids: Science and Technology*; John Wiley & Sons: Hoboken, NJ, USA, 2008.
107. Kuo, K.K.; Risha, G.A.; Evans, B.J.; Boyer, E. Potential Usage of Energetic Nano-sized Powders for Combustion and Rocket Propulsion. *MRS Online Proc. Libr.* **2003**, *800*, 39–50. [CrossRef]
108. Yanaoka, H.; Inafune, R. Frequency response of three-dimensional natural convection of nanofluids under microgravity environments with gravity modulation. *Numer. Heat Transf. Part A Appl.* **2023**, *83*, 745–769. [CrossRef]
109. Mohammed, H.I.; Giddings, D.; Walker, G.S.; Talebizadehsardari, P.; Mahdi, J.M. Thermal behaviour of the flow boiling of a complex nanofluid in a rectangular channel: An experimental and numerical study. *Int. Commun. Heat Mass Transf.* **2020**, *117*, 104773. [CrossRef]
110. Chen, Y.; Li, X.; Fang, X.; He, Z.; Fang, Y. Experimental Investigation of Critical Heat Flux of Nucleate Pool Boiling of Water and Nanofluid on Platinum Wire Under Hypergravity and Earth Gravity. *Microgravity Sci. Technol.* **2023**, *35*, 61. [CrossRef]
111. Arif, M.; Kumam, P.; Kumam, W.; Mostafa, Z. Heat transfer analysis of radiator using different shaped nanoparticles water-based ternary hybrid nanofluid with applications: A fractional model. *Case Stud. Therm. Eng.* **2022**, *31*, 101837. [CrossRef]
112. Henein, S.M.; Abdel-Rehim, A.A. The performance response of a heat pipe evacuated tube solar collector using MgO/MWCNT hybrid nanofluid as a working fluid. *Case Stud. Therm. Eng.* **2022**, *33*, 101957. [CrossRef]
113. Wu, W.-C.; Kumar, A. Numerical Investigation of Nanofluid Flow over a Backward Facing Step. *Aerospace* **2022**, *9*, 499. [CrossRef]
114. Chen, C.; Feng, S.; Peng, H.; Peng, X.; Chaoyue, L.; Zhang, R. Thermocapillary Convection Flow and Heat Transfer Characteristics of Graphene Nanoplatelet Based Nanofluid Under Microgravity. *Microgravity Sci. Technol.* **2021**, *33*, 40. [CrossRef]
115. Zhang, B.; Tang, L.; Zhang, H.; Ali, B.; Shah, N.A.; Jeon, Y. Finite element study of nanoparticles spacing and radius on dynamics of water fluid subject to microgravity environment. *Results Phys.* **2023**, *47*, 106355. [CrossRef]
116. Dong, S.; Jiang, H.; Xie, Y.; Wang, X.; Zhu, Z.; Wang, J. Experimental investigation on boiling heat transfer characteristics of Al_2O_3-water nanofluids in swirl microchannels subjected to an acceleration force. *Chin. J. Aeronaut.* **2019**, *32*, 1136–1144. [CrossRef]
117. Wu, X.; Ye, D.; Jin, S.; He, G.; Guo, Y.; Fang, W. Cracking of platinum/hydrocarbon nanofluids with hyperbranched polymer as stabilizer and initiator. *Fuel* **2019**, *255*, 115782. [CrossRef]
118. Hussain, S.M. Dynamics of radiative Williamson hybrid nanofluid with entropy generation: Significance in solar aircraft. *Sci. Rep.* **2022**, *12*, 8916. [CrossRef] [PubMed]
119. Khan, U.; Ahmed, N.; Mohyud-Din, S.T.; Alsulami, M.D.; Khan, I. A novel analysis of heat transfer in the nanofluid composed by nanodimaond and silver nanomaterials: Numerical investigation. *Sci. Rep.* **2022**, *12*, 1284. [CrossRef]
120. Jamshed, W. Thermal augmentation in solar aircraft using tangent hyperbolic hybrid nanofluid: A solar energy application. *Energy Environ.* **2022**, *33*, 1090–1133. [CrossRef]
121. Salawu, S.O.; Obalalu, A.M.; Shamshuddin, M. Nonlinear Solar Thermal Radiation Efficiency and Energy Optimization for Magnetized Hybrid Prandtl–Eyring Nanoliquid in Aircraft. *Arab. J. Sci. Eng.* **2023**, *48*, 3061–3072. [CrossRef]

122. Jamshed, W.; Alanazi, A.K.; Isa, S.S.P.M.; Banerjee, R.; Eid, M.R.; Nisar, K.S.; Alshahrei, H.; Goodarzi, M. Thermal efficiency enhancement of solar aircraft by utilizing unsteady hybrid nanofluid: A single-phase optimized entropy Analysis. *Sustain. Energy Technol. Assess.* **2022**, *52 Pt A*, 101898. [CrossRef]
123. Meyyappan, M. Nanotechnology in Aerospace Applications. In *Educational Notes RTO-EN-AVT-129*; RTO: Neuilly-sur-Seine, France, 2005; Volume 6, pp. 1–2.
124. Raghu, S. Microfluidics for Aerospace Applications. In *Microfluidics and Nanofluidics Handbook: Fabrication, Implementation, and Applications*; Mitra, S.K., Chakraborty, S., Eds.; CRC Press: Boca Raton, FL, USA, 2012. [CrossRef]
125. Kuang, S.; Singh, N.M.; Wu, Y.; Shen, Y.; Ren, W.; Tu, L.; Yong, K.T.; Song, P. Role of microfluidics in accelerating new space missions. *Biomicrofluidics* **2022**, *16*, 021503. [CrossRef]
126. Krakos, A. Lab-on-chip technologies for space research—current trends and prospects. *Microchim. Acta* **2023**, *191*, 31. [CrossRef] [PubMed]
127. Cinti, S.; Singh, S.; Covone, G.; Tonietti, L.; Ricciardelli, A.; Cordone, A.; Iacono, R.; Mazzoli, A.; Moracci, M.; Rotundi, A.; et al. Reviewing the state of biosensors and lab-on-a- chip technologies: Opportunities for extreme environments and space exploration. *Front. Microbiol.* **2023**, *14*, 1215529. [CrossRef] [PubMed]
128. Low, L.A.; Giulianotti, M.A. Tissue Chips in Space: Modeling Human Diseases in Microgravity. *Pharm. Res.* **2019**, *37*, 8. [CrossRef] [PubMed]